IEEE Access
Multidisciplinary ⋮ Rapid Review ⋮ Open Access Journal

Received 6 December 2023, accepted 14 December 2023, date of publication 18 December 2023, date of current version 21 December 2023.

Digital Object Identifier 10.1109/ACCESS.2023.3343914

RESEARCH ARTICLE

Proposing a BSPID Control Strategy Considering External Disturbances for Electric Power Steering (EPS) Systems

DUC NGOC NGUYEN AND TUAN ANH NGUYEN
Automotive Engineering Department, Thuyloi University, Hanoi 100000, Vietnam
Corresponding author: Tuan Anh Nguyen (anhngtu@tlu.edu.vn)

ABSTRACT EPS systems provide superior efficiency compared to mechanical steering systems. Steering feel and comfort are supported by an electric motor, which is controlled by an appropriate controller. This article introduces an integrated control algorithm for the EPS system with two novel contributions. Firstly, this algorithm is synthesized based on a backstepping (BS) controller and a proportional integral derivative (PID) controller, called the BSPID controller. The control signals are amplified based on optimal coefficients determined by the loop algorithm. Secondly, a complex steering dynamics model is established based on five state variables that consider the influence of road reaction torque and other external disturbances. According to numerical simulation results, the value of the steering motor and steering column angles increases when using the EPS system instead of the conventional steering system. Under the same driver torque conditions, the variation of output parameters will decrease as the speed increases. On the contrary, the change in output parameters will increase sharply when driver torque increases (under the same speed conditions). The results obtained from the BSPID signal always closely track the reference signal in all investigated conditions with negligible errors, even though the steering system is still subject to external random disturbances.

INDEX TERMS Backstepping control, PID control, EPS system, simulation, assisted torque, driver torque.

NOMENCLATURE

Symbol	Description	Unit
δ	Steering angle	rad.
ψ	Yaw angle	rad.
β	Heading angle	rad.
α	Slip angle	rad.
θ_c	Steering column angle	rad.
θ_m	Steering motor angle	rad.
γ_c	Camber angle	rad.
γ_k	Kingpin angle	rad.
B_c	Steering column damping coefficient	Nms/rad.
B_{eq}	Equivalent damping coefficient	Nms/rad.
B_m	Motor shaft damping coefficient	Nms/rad.
B_r	Damping coefficient of the rack	Ns/m.
C_α	Cornering stiffness coefficient	N/rad.
F_c	Steering column friction coefficient	Nm.
F_{ex}	External longitudinal force	N.
F_{ey}	External lateral force	N.
F_{ix}	Internal longitudinal force	N.
F_{iy}	Internal lateral force	N.
F_m	Motor friction coefficient	Nm.
i	Motor ratio	-.
i_m	Motor current	A.
J_c	Steering column moment of inertia	kgm^2.
J_{eq}	Equivalent moment of inertia	kgm^2.
J_m	Steering motor moment of inertia	kgm^2.
J_z	Yaw moment of inertia	kgm^2.
K_c	Steering column stiffness	Nm/rad.
K_r	Tire spring rate	N/mrad.
K_t	Motor torque coefficient	Nm/A.
l_c	Caster trail	m.
L_m	Motor inductance	H.

The associate editor coordinating the review of this manuscript and approving it for publication was Jjun Cheng.

l_n	Length of the knuckle arm	m.
m	Vehicle mass	kg.
M_{ez}	External aligning moment	Nm.
M_{iz}	Internal aligning moment	Nm.
M_r	Mass of the rack	kg.
R_m	Motor resistance	Ω.
r_p	Pinion radius	m.
T_a	Assisted torque	Nm.
T_d	Driver torque	Nm.
T_{ed}	External disturbances	Nm.
T_r	Road reaction torque	Nm.
$u(t)$	Control signal	V.
v_x	Longitudinal velocity	m/s.
v_y	Lateral velocity	m/s.

I. INTRODUCTION

The steering system plays an essential role in controlling the direction of motion and ensuring the car's stability. Nowadays, most vehicles use the power steering system instead of the conventional mechanical one. The power steering system supports assisted torque for the driver during steering. Therefore, the driving process becomes easier and more comfortable.

There are three types of power steering systems commonly used today: electric power steering (EPS), hydraulic power steering (HPS), and electrohydraulic power steering (EHPS) systems [1]. The HPS system is often used on trucks or old passenger vehicles. The structure of HPS and EHPS systems is quite bulky, including a hydraulic pump, a reservoir, valve systems, and oil pipelines [2]. The hydraulic pump is continuously driven by the engine (for HPS systems). Therefore, it consumes much power even when the car goes straight. The opening and closing process of hydraulic valves has an unavoidable delay and fluid friction still exists, which causes a loss of performance. In addition, the stability performance of the HPS system when the car moves at high speed is not good. As a result, HPS and EHPS systems should be replaced by EPS systems. In [3], Baharom et al. pointed out some advantages of the EPS system, such as being less complicated, environmentally friendly, and more energy efficient. According to Jang et al., the EPS system performed better than the hydraulic steering system, while the electric motor was vibrationless and quiet [4]. The EPS system could support the driver in most situations based on extreme dynamics with high precision and comfortable operation, according to Truemmel et al. [5]. EPS systems could be used on many types of vehicles, including pickups, minivans, sedans, hatchbacks, sport utility vehicles (SUVs), crossover utility vehicles (CUVs), etc. [6]. According to Chung and Lee, the EPS system was relatively compact, so it could be arranged in many locations, such as the EPS column, EPS rack, EPS pinion, and dual EPS pinion (see Figure 1 in [7]). Electric power steering systems could be combined with electronic suspension systems [8] or modern autonomous vehicle technologies [9], [10]. The general goal of the EPS system was to reduce driver torque for the user (improve comfort) while still ensuring steering feel [11].

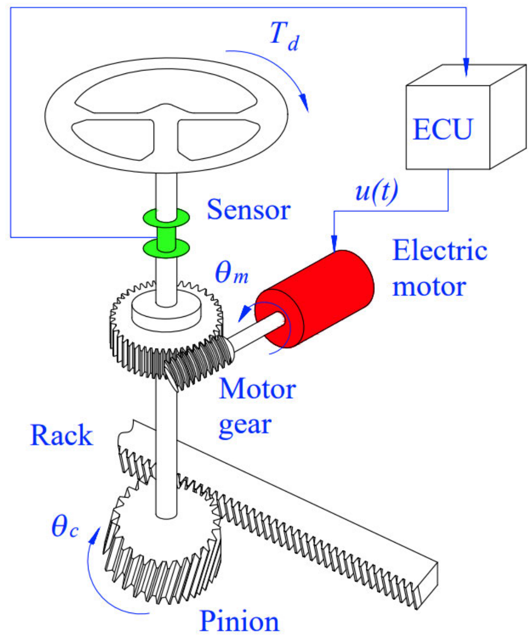

FIGURE 1. EPS model.

The EPS system usually includes main components such as a steering wheel, steering column, steering gear box (rack and pinion, worm and ball nut, etc.), sensors, electric motor, electronic control unit (ECU), and steering bars (see Figure 1). In particular, the electric motor and ECU are the two most essential components of the steering system. Electric motors usually use a 12 V voltage with a 1 ÷ 2 Nm rated torque. However, the specifications of different devices are different. The characteristic curve of assisted torque can be a saturated straight line [12], [13] or a nonlinear curve [14], [15]. The power steering characteristic curve depends on speed and driver torque. Some articles showed that the change in the characteristic curve also depended on the adhesion coefficient [12], [13]. The performance of the electric motor depends on the control algorithm previously designed for the system.

To simplify the control problem, the EPS system is considered linear. Therefore, classical control algorithms can be used to control this system. In [16], Chen et al. introduced the use of a simple PI controller for the EPS system. The coefficients of this controller were selected as follows: $k_P = 20400$ and $k_I = 700$. A full PID controller was established in [11] by Guan et al. According to Guan et al., the input to the controller was steering style (driver torque), while the output was desired assisted torque. The parameters of the PID controller could be optimally calculated using the ant colony optimization (ACO) algorithm [17] or particle swarm optimization (PSO) [18]. These algorithms were generally global instead of local, like the genetic algorithm (GA) [19]. Besides, these parameters could also be optimally calculated using loop algorithms [20], [21]. The optimal values were fixed in all situations. Therefore, they were only suitable for specific conditions mentioned in the optimal algorithm. To help the system adapt to many conditions, Zheng and Wei proposed using a fuzzy algorithm for the PI controller [22]. The fuzzy algorithm in [22] had two membership functions, in which the membership functions of coefficients k_P and k_I were built based on triangular functions. In [23], Nguyen used Gaussian functions to design membership functions for PI controllers. Another form of the membership function used to adjust the parameters for a PID controller was shown in [24]. For systems with multiple outputs and multiple inputs, a linear quadratic regulator (LQR) was a suitable choice instead of PID. A Gaussian filter was combined with the LQR control technique to become LQG [25]. In cases where the system was subject to the influence of external disturbances, we could design a linearly expanding observer to improve the system's performance [26].

In fact, the motion of the electric power steering system is nonlinear. Therefore, using control algorithms for nonlinear systems can bring higher efficiency. In [27], Lee et al. indicated that results could not converge when only using a linear controller for the EPS system. In [28], Zhao et al. proved that the H_∞ algorithm controlled the signal response more efficiently than PID. If we used the regular H_2 algorithm, its performance would be lower than PID in some cases, according to Zhao et al. [28]. To solve this problem, Zhao et al. introduced a combination between H_2 and H_∞ in [29]. Another performance comparison between H_∞ and PID could be found in [30]. In [31], Nasri et al. claimed that H_∞ static output feedback (SOF) control could solve several practical problems relating to measuring the values of the friction coefficient, the slip angle, and disturbances. The algorithm in [31] was based on the Takagi-Sugeno (T-S) fuzzy model via Lyapunov functions. In [32], Lee et al. designed an ESP system's sliding mode control (SMC) solution. This technique was founded on the Lyapunov stability principle. The controlled object was the steering wheel torque. The SMC technique required taking the higher-order derivative of the object and designing a suitable sliding surface [33], [34], and [35]. The results in [32], [36] showed that the chattering phenomenon still occurred when applying this technique to EPS systems. This characteristic phenomenon of the SM algorithm should be eliminated (see [37], [38], [39], [40]). Different from [32], the controlled objects in [41] and [42] were sensed steering torque and pinion angle, respectively. To accomplish this goal, Lee et al. established a torque feedback controller with two modules: the steering feel module and the steering torque module [41], while Jeong et al. used a hybrid nonlinear controller [42].

During the operation, the EPS system could be subject to many external influences, such as crosswind [43], roughness on the road, etc., commonly referred to as disturbances. To improve system performance, Ma et al. introduced an active disturbance reject control method for the EPS system [44]. External disturbances could be rejected using Gaussian and Kalman filters, according to Mehrabi et al. [45]. In some extreme conditions, we were able to use the active disturbance rejection control (ADRC) method to apply it to the steering system. This method was designed by Zheng and Wei in [46]. A control solution might compensate for friction in EPS systems, as shown in [47] by Wilhelm et al. Besides, the system's torque oscillation would affect stability. This problem could be solved using the two-loop algorithm (the torque loop and current loop) in [48]. Some nonlinear control methods for EPS systems should be found in [49], [50], [51], [52], and [53].

Many integrated intelligent control methods should be applied to the steering system to ensure the criteria of steering feel and system stability. In [54], Hung et al. used the wavelet fuzzy neural network method to control the EPS system. The membership functions of this controller were designed asymmetrically, according to Hung et al. However, the specific content of the membership functions was not clearly presented. In [55], Saifia et al. introduced a T-S fuzzy algorithm to represent the nonlinear dynamic behavior of an EPS system model. The findings in [56] demonstrated that the fuzzy algorithm-controlled signal followed the reference signal more closely than PID. In [57], Fu et al. designed a robust fuzzy algorithm with two layers for the steering system. However, the variation of the dynamic parameters was not shown in [57]. Abnormalities in the operation of the EPS system should be detected early based on deep learning applications, according to Alabe et al. [58]. Some other intelligent control applications for EPS systems were shown in [59], [60], [61], [62], and [63].

The research results could be evaluated in the frequency domain [64] or the time domain [55], [56]. Many dynamic models were used to describe the motion of EPS systems. Their complexity depended on the controlled objective [17], [18], [65], [66]. Generally, these models often ignored the determination of road reaction torque (T_r). In [66], Murilo et al. assumed that the rectangular pulse signals predetermined the value of T_r. In [67], Jang et al. proposed a modeling method for road reaction torque. A more straightforward method of calculating T_r was shown in [55] by Saifia et al. In conclusion, consideration of the influence of road reaction torque is necessary. In addition, the influence of external disturbances, such as crosswinds, roughness on the road, etc., should also be mentioned.

The above control techniques all achieve high efficiency under certain conditions. However, some technical issues still exist and should be resolved. Firstly, the motion of the electric power steering system is nonlinear. This is caused by many reasons, including user reaction (driver torque), road reaction torque, other external disturbances (crosswind, roughness on the road), the car's and steering system's structure (including the influence of the tire and the suspension system), and other factors. In addition, the steering system and motion models are established based on nonlinear equations, making the problem more complicated. Therefore, the system should be controlled by robust nonlinear control algorithms such as H_∞, SMC, BS, etc., instead of just using simple classical algorithms (PID, LQR, LQG). Secondly, the chattering phenomenon still occurs when using nonlinear control algorithms (such as SMC) for the steering system. This is a significant drawback that needs to be thoroughly resolved. Thirdly, intelligent control algorithms and artificial intelligence applications are quite complex. We can use integrated nonlinear algorithms instead of designing complicated control applications. Finally, the value of road reaction torque should be carefully calculated based on the car dynamics model. In addition, the influence of external disturbances should also be considered.

For these reasons, we propose designing an integrated nonlinear control algorithm. This new algorithm combines the backstepping (BS) method and PID control, called BSPID. This algorithm can take advantage of the advantages of BS and PID techniques, such as high reliability and systematicity (PID), good stability and response against nonlinear changes (BS), the limitation of chattering phenomena that occur when using a nonlinear algorithm (BS), and other advantages. In addition, the influence of road reaction torque and other external disturbances is also considered when designing the EPS system model, which is fully described through the complex dynamic model. These are two new contributions to the article that have never been made in previous studies (previous articles often used only a single PID or BS algorithm for the EPS system instead of an integrated control technique. Some integrated control applications between PID and BS or SMC were often only used to control other automotive mechatronic systems, such as suspension or braking systems, instead of steering systems. In addition, many publications on EPS control often assumed that the value of the road reaction torque was known and the influence of other external disturbances was ignored). The content of this article is divided into four sections: the introduction section, the mathematical model section, the results and discussion section, and the conclusion section. The process of designing the EPS system model, vehicle motion model, and control algorithm is carried out in the second section.

II. MATHEMATICAL MODEL

A. EPS SYSTEM MODEL

The EPS system model is illustrated in Figure 1. The mechanical principle of the EPS system is described by equations (1) and (2) according to Newton's law.

$$J_c\ddot{\theta}_c + B_c\dot{\theta}_c + F_c sgn\left(\dot{\theta}_c\right) + K_c\theta_c - \frac{K_c}{i}\theta_m = T_d \tag{1}$$

$$\frac{K_c}{i}\theta_c - J_{eq}\ddot{\theta}_m - F_m sgn\left(\dot{\theta}_m\right) - B_{eq}\dot{\theta}_m - \frac{K_c + K_r r_p^2}{i^2}\theta_m = \frac{T_r}{i} - K_t i_m \tag{2}$$

The control current i_m in equation (2) is determined according to (3).

$$L_m\dot{i}_m + R_m i_m = u\left(t\right) - K_t\dot{\theta}_m \tag{3}$$

where:

$$J_{eq} = J_m + \frac{r_p^2}{i^2}M_r \tag{4}$$

$$B_{eq} = B_m + \frac{r_p^2}{i^2}B_r \tag{5}$$

Ignoring $sgn(.)$ functions in equations (1) and (2) [66], substituting equations (4) and (5) into the first two equations, we get:

$$J_c\ddot{\theta}_c + B_c\dot{\theta}_c + K_c\theta_c - \frac{K_c}{i}\theta_m = T_d \tag{6}$$

$$\frac{K_c}{i}\theta_c - \left(J_m + \frac{r_p^2}{i^2}M_r\right)\ddot{\theta}_m - \left(B_m + \frac{r_p^2}{i^2}B_r\right)\dot{\theta}_m - \frac{K_c + K_r r_p^2}{i^2}\theta_m = \frac{T_r}{i} - K_t i_m \tag{7}$$

T_d is the input to differential equations, while T_r is an unknown (road reaction torque). The value of T_r can be calculated through a linear single-track dynamic model. According to [68], the forces and moments acting on the car are described as follows:

$$m\left(\dot{v}_x - \dot{\psi}v_y\right) = F_{x1} + F_{x2} \tag{8}$$

$$m\left(\dot{v}_y + \dot{\psi}v_x\right) = F_{y1} + F_{y2} \tag{9}$$

$$J_z\ddot{\psi} = l_1F_{y1} - l_2F_{y2} \tag{10}$$

Assuming that the steering angle is small (*), the tire's lateral force is considered linear. As a result, the product between the slip angle and the cornering stiffness determines the value of F_y.

$$F_{y1} = -C_{\alpha1}\alpha_1 \tag{11}$$

$$F_{y2} = -C_{\alpha2}\alpha_2 \tag{12}$$

where:

$$\alpha_1 = \beta_1 - \delta = \frac{v_y + l_1\dot{\psi}}{v_x} - \delta \tag{13}$$

$$\alpha_2 = \beta_2 = \frac{v_y - l_2\dot{\psi}}{v_x} \tag{14}$$

If a car moves at a constant speed (**), equation (8) will disappear. Combining equations from (9) to (12), we get:

$$\dot{v}_y = \frac{1}{mv_x}\left(-l_1C_{\alpha1} + l_2C_{\alpha2} - mv_x^2\right)\dot{\psi} - \frac{1}{mv_x}\left(C_{\alpha1} + C_{\alpha2}\right)v_y + \frac{1}{m}C_{\alpha1}\delta \tag{15}$$

$$\ddot{\psi} = \frac{1}{J_zv_x}\left(-l_1^2C_{\alpha1} - l_2^2C_{\alpha2}\right)\dot{\psi} - \frac{1}{J_zv_x}\left(l_1C_{\alpha1} - l_2C_{\alpha2}\right)v_y + \frac{1}{J_z}l_1C_{\alpha1}\delta \tag{16}$$

where: the vehicle heading angle β is determined according to (17).

$$\beta = arctan\frac{v_y}{v_x} \tag{17}$$

Combining conditions (*) and (**), we obtain an approximate equation like (18).

$$\dot{v}_y \approx v_x\dot{\beta} \tag{18}$$

Combining (15), (16), and (18), the car's motion can be described as a state matrix as below.

$$\begin{bmatrix} \dot{\beta} \\ \ddot{\psi} \end{bmatrix} = A\begin{bmatrix} \beta \\ \dot{\psi} \end{bmatrix} + B[\delta] \tag{19}$$

where:

$$A = \begin{bmatrix} -\dfrac{C_{\alpha 1}+C_{\alpha 2}}{mv_x} & -\dfrac{l_1C_{\alpha 1}-l_2C_{\alpha 2}+mv_x^2}{mv_x^2} \\ -\dfrac{l_1C_{\alpha 1}-l_2C_{\alpha 2}}{J_z} & -\dfrac{l_1^2C_{\alpha 1}+l_2^2C_{\alpha 2}}{J_zv_x} \end{bmatrix}$$

$$B = \begin{bmatrix} \dfrac{C_{\alpha 1}}{mv_x} & \dfrac{l_1C_{\alpha 1}}{J_z} \end{bmatrix}^T$$

According to [69], the road reaction torque can be approximated as equation (20).

$$T_r \approx l_cr_p\frac{cos^2(\gamma_k)\,cos^2(\gamma_c)}{l_n}F_{y1} \tag{20}$$

The symbols used in equations from (1) to (20) can be referred to in the Nomenclature section.

B. CONTROL SYSTEM MODEL

In this study, we establish a nonlinear control algorithm called backstepping control for the EPS system. This algorithm is designed based on the Lyapunov stability theory.

Set state variables as follows:

$$x_1 = \theta_c \tag{21}$$
$$x_2 = \dot{\theta}_c \tag{22}$$
$$x_3 = \theta_m \tag{23}$$
$$x_4 = \dot{\theta}_m \tag{24}$$
$$x_5 = i_m \tag{25}$$

Taking the derivative of the state variables from x_1 to x_5, we get:

$$\dot{x}_1 = x_2 \tag{26}$$
$$\dot{x}_2 = -\frac{K_c}{J_c}x_1 - \frac{B_c}{J_c}x_2 + \frac{K_c}{J_ci}x_3 + \frac{T_d}{J_c} \tag{27}$$
$$\dot{x}_3 = x_4 \tag{28}$$
$$\dot{x}_4 = \frac{K_c}{J_{eq}i}x_1 - \frac{K_c+K_rr_p^2}{J_{eq}i^2}x_3 - \frac{B_{eq}}{J_{eq}}x_4 + \frac{K_t}{J_{eq}}x_5 - \frac{T_r}{J_{eq}i} \tag{29}$$
$$\dot{x}_5 = -\frac{K_t}{L_m}x_4 - \frac{R_m}{L_m}x_5 + \frac{1}{L_m}u(t) \tag{30}$$

Let e_1 be the error between the controlled signal (x_3) and the desired result (x_{ref}):

$$e_1 = x_3 - x_{ref} \tag{31}$$

Let e_2 and e_3 be virtual errors of the system:

$$e_2 = x_4 - \lambda_1 \tag{32}$$
$$e_3 = x_5 - \lambda_2 \tag{33}$$

where: λ is a virtual control variable.

Taking the derivative of equation (31), we get (34).

$$\dot{e}_1 = \dot{x}_3 - \dot{x}_{ref} = x_4 - \dot{x}_{ref} \tag{34}$$

The virtual control variable λ_1 is selected according to (35) to satisfy condition (36).

$$\lambda_1 = -c_1e_1 + \dot{x}_{ref} \tag{35}$$
$$e_2 = x_4 - \lambda_1 = x_4 + c_1e_1 - \dot{x}_{ref} = \dot{e}_1 + c_1e_1 \xrightarrow{e_1\approx 0} \dot{e}_1 \tag{36}$$

Combining (32), (34), and (35), we obtain equation (37).

$$\dot{e}_1 = e_2 - c_1e_1 \tag{37}$$

Combining the derivative of (32) and equation (35), we get (38).

$$\begin{aligned}\dot{e}_2 &= \dot{x}_4 - \dot{\lambda}_1 = \dot{x}_4 - \left(-c_1\dot{e}_1 + \ddot{x}_{ref}\right) \\ &= \dot{x}_4 + c_1(e_2 - c_1e_1) - \ddot{x}_{ref}\end{aligned} \tag{38}$$

Equation (39) is established by substituting (29) into (38).

$$\begin{aligned}\dot{e}_2 = \frac{K_c}{J_{eq}i}x_1 - \frac{K_c+K_rr_p^2}{J_{eq}i^2}x_3 - \frac{B_{eq}}{J_{eq}}x_4 + \frac{K_t}{J_{eq}}x_5 \\ - \frac{T_r}{J_{eq}i} + c_1e_2 - c_1^2e_1 - \ddot{x}_{ref}\end{aligned} \tag{39}$$

Substituting (32) and (35) into (39), we get (40), as shown at the bottom of the next page, where:

$$c_2 = \frac{B_{eq}}{J_{eq}} - c_1 \tag{41}$$

Take the derivative of (33):

$$\dot{e}_3 = \dot{x}_5 - \dot{\lambda}_2 \tag{42}$$

The virtual control variable λ_2 is selected according to (43).

$$\lambda_2 = K_1x_{ref} \tag{43}$$

where: K_1 is a scaling factor between x_5 and x_{ref}.

Combining (30), (42), and (43), we get (44).

$$\begin{aligned}\dot{e}_3 &= -\frac{K_t}{L_m}x_4 - \frac{R_m}{L_m}x_5 + \frac{1}{L_m}u(t) - K_1\dot{x}_{ref} \\ &= -\frac{K_t}{L_m}x_4 - \frac{R_m}{L_m}(e_3+\lambda_2) + \frac{1}{L_m}u(t) - K_1\dot{x}_{ref} \\ &= \underbrace{-\frac{K_t}{L_m}x_4 - K_1\frac{R_m}{L_m}x_{ref} - K_1\dot{x}_{ref}}_{f_2(x)} + \frac{1}{L_m}u(t) - \frac{R_m}{L_m}e_3\end{aligned}$$

$$=f_2(x)+\frac{1}{L_m}u(t)-\frac{R_m}{L_m}e_3 \tag{44}$$

The Lyapunov function is selected as in equation (45). The function $V(x)$ is always positive-definite $\forall x \neq 0$.

$$V=\frac{1}{2}e_1^2+\frac{1}{2}e_2^2+\frac{1}{2}e_3^2>0 \quad \forall x\neq 0 \tag{45}$$

Taking the derivative of (45), we get (46).

$$\dot{V}=e_1\dot{e}_1+e_2\dot{e}_2+e_3\dot{e}_3 \tag{46}$$

Substituting equations (37), (40), and (44) into (46), we get:

$$\begin{aligned}\dot{V}&=e_1(e_2-c_1e_1)+e_2(f_1(x)-c_2e_2)\\&\quad+e_3\left(f_2(x)+\frac{1}{L_m}u(t)-\frac{R_m}{L_m}e_3\right)\\&=e_1e_2-c_1e_1^2+e_2f_1(x)-c_2e_2^2+e_3f_2(x)\\&\quad-\frac{R_m}{L_m}e_3^2+\frac{e_3}{L_m}u(t)\\&=\left(-c_1e_1^2-c_2e_2^2-c_3e_3^2\right)\\&\quad+\left(e_1e_2+e_2f_1(x)+e_3f_2(x)+\frac{e_3}{L_m}u(t)\right)\end{aligned} \tag{47}$$

where:

$$c_3=\frac{R_m}{L_m} \tag{48}$$

The control signal $u(t)$ is selected according to (49).

$$\begin{aligned}u(t)&=-L_m\left(\frac{e_2(e_1+f_1(x))}{e_3}+f_2(x)\right)\\&=-L_m(f_3(x)f_4(x)+f_2(x))\end{aligned} \tag{49}$$

where:

$$\begin{aligned}&f_3(x)\\&=\frac{e_2}{e_3}=\frac{c_1x_3+x_4-c_1x_{ref}-\dot{x}_{ref}}{x_5-K_1x_{ref}}\end{aligned} \tag{50}$$

$$\begin{aligned}&f_4(x)\\&=e_1+f_1(x)\\&=\frac{K_c}{J_{eq}i}x_1+\left(c_1\frac{B_{eq}}{J_{eq}}-\frac{K_c+K_rr_p^2}{J_{eq}i^2}+1-c_1^2\right)x_3+\frac{K_t}{J_{eq}}x_5\\&\quad+\left(-\frac{c_1B_{eq}+J_{eq}\left(1+c_1^2\right)}{J_{eq}}x_{ref}-\frac{B_{eq}}{J_{eq}}\dot{x}_{ref}-\ddot{x}_{ref}\right)-\frac{T_r}{J_{eq}i}\end{aligned} \tag{51}$$

Substituting equations (49), (50), and (51) into (47), we obtain equation (52).

$$\dot{V}=-c_1e_1^2-c_2e_2^2-c_3e_3^2<0 \quad \forall c_3,\ 0<c_1<\frac{B_{eq}}{J_{eq}} \tag{52}$$

According to Lyapunov theory, a system is considered stable when its control Lyapunov function (CLF) is positive-definite and its derivative is negative-definite. The results in (45) and (52) show that the system is always stable when applying the backstepping algorithm to the EPS system model.

Calculating the value of the function $f_3(x)$ in equation (50) is quite complicated. Therefore, we propose a method to approximate this function as follows:

According to the initial simulation results, the RMS value of e_2 is proportional to e_3, therefore:

$$f_3=\frac{RMS(e_2)}{RMS(e_3)}\approx K_2 \tag{53}$$

With: K_2 is the scaling factor determined by computational simulation.

Substituting equations (31), (32), (33), (36), and (43) into equation (53), we obtain equation (54).

$$\begin{aligned}&c_1x_3+x_4-c_1x_{ref}-\dot{x}_{ref}\\&=K_2\left(x_5-K_1x_{ref}\right)\\&\Leftrightarrow c_1\left(x_3-x_{ref}\right)+K_3\left(x_3-x_{ref}\right)=K_2K_4\left(x_3-x_{ref}\right)\\&\Leftrightarrow \left(x_3-x_{ref}\right)(c_1+K_3-K_2K_4)=0\end{aligned} \tag{54}$$

With: K_3 is the scaling factor between (x_3-x_{ref}) and its derivative; K_4 is the scaling factor between (x_3-x_{ref}) and $(x_5-K_1x_{ref})$.

Assuming that (x_3-x_{ref}) is only approximately equal to zero, the solution of equation (54) is determined as follows:

$$K_2=\frac{c_1+K_3}{K_4} \tag{55}$$

$$\begin{aligned}\dot{e}_2&=\frac{K_c}{J_{eq}i}x_1-\frac{K_c+K_rr_p^2}{J_{eq}i^2}x_3-\frac{B_{eq}}{J_{eq}}(e_2+\lambda_1)+\frac{K_t}{J_{eq}}x_5-\frac{T_r}{J_{eq}i}+c_1e_2-c_1^2e_1-\ddot{x}_{ref}\\&=\frac{K_c}{J_{eq}i}x_1-\frac{K_c+K_rr_p^2}{J_{eq}i^2}x_3-\frac{B_{eq}}{J_{eq}}\left(-c_1e_1+\dot{x}_{ref}\right)+\frac{K_t}{J_{eq}}x_5-\frac{T_r}{J_{eq}i}+\left(c_1-\frac{B_{eq}}{J_{eq}}\right)e_2-c_1^2e_1-\ddot{x}_{ref}\\&=\frac{K_c}{J_{eq}i}x_1-\frac{K_c+K_rr_p^2}{J_{eq}i^2}x_3+c_1\frac{B_{eq}}{J_{eq}}\left(x_3-x_{ref}\right)-\frac{B_{eq}}{J_{eq}}\dot{x}_{ref}+\frac{K_t}{J_{eq}}x_5-\frac{T_r}{J_{eq}i}+\left(c_1-\frac{B_{eq}}{J_{eq}}\right)e_2-c_1^2e_1-\ddot{x}_{ref}\\&=\underbrace{\frac{K_c}{J_{eq}i}x_1+\left(c_1\frac{B_{eq}}{J_{eq}}-\frac{K_c+K_rr_p^2}{J_{eq}i^2}\right)x_3+\frac{K_t}{J_{eq}}x_5+\left(-c_1\frac{B_{eq}}{J_{eq}}x_{ref}-\frac{B_{eq}}{J_{eq}}\dot{x}_{ref}-\ddot{x}_{ref}\right)+\left(-\frac{T_r}{J_{eq}i}-c_1^2e_1\right)}_{f_1(x)}-c_2e_2\\&=f_1(x)-c_2e_2\end{aligned} \tag{40}$$

Substituting equations (44), (51), and (53) into equation (49), we get (56), as shown at the bottom of the page.

In this study, we propose to use an integrated controller called BSPID, which combines backstepping (BS) and PID. There are two main reasons for this choice. Firstly, system stability will not be guaranteed under extreme conditions if only a single PID controller is used. In addition, the system's responsiveness is not high. Secondly, if we only use a single BS controller, the output signal (controlled object) will be delayed compared to the desired signal (this has been verified through many simulations before). The second problem can be overcome by selecting PID controller coefficients, while the first problem can be solved by applying the BSC technique. Therefore, the combination of these two techniques is a good idea. The control signal in equation (56) is the first control signal of the controller. Therefore, $u(t) = u_1(t)$. The second control signal is determined by the PID controller according to equation (57).

$$u_2(t) = k_P e_4 + k_I \int e_4 dt + k_D \dot{e}_4 \tag{57}$$

where: k_P, k_I, and k_D are the controller coefficients, and e_4 is the error between the reference signal and the output result.

$$e_4 = x_3 - x_{ref} \tag{58}$$

The final control signal is synthesized from the signals $u_2(t)$ and $u_1(t)$ in equation (59). The coefficients a_1 and a_2 are optimally calculated by a loop algorithm to ensure controller performance.

$$u(t) = a_1 u_1(t) + a_2 u_2(t) \tag{59}$$

The loop optimization calculation process includes two steps. The raw optimal values are found in the first step. The value of a_1 is in the range from a_{1min} to a_{1max}, while the value of a_2 is from a_{2min} to a_{2max}. By using manual calculation and their boundary conditions, one can determine the values of a_{min} and a_{max}. The smallest steps (m and n) should be chosen accordingly. If the values of m and n are too large, the error will increase. On the contrary, if the values of m and n are too small, the calculation time will be extremely long. The program stops only once it has gone through all the values within this limit, corresponding to the smallest steps. The raw optimal value is chosen so the system error is minimal, $e(t) = e(t)_{min}$.

$$\left\{\begin{array}{l} for \begin{cases} a_{1\_raw} = a_{1\_min} : m : a_{1\_max} \\ a_{2\_raw} = a_{2\_min} : n : a_{2\_max} \end{cases} \\ if \;\; e(t) = e(t)_{min} \\ \quad \begin{cases} a_{1\_raw\_optimal} = a_{1\_raw} \\ a_{2\_raw\_optimal} = a_{2\_raw} \end{cases} \\ else \begin{cases} a_{1\_raw\_optimal} = a_{1\_raw+m} \\ a_{2\_raw\_optimal} = a_{2\_raw+n} \end{cases} \end{array}\right\} \tag{60}$$

The second step of the optimization calculation will be performed after we have found the raw optimal values. Like the first step (60), calculating the acceptable optimization is indicated in (61). The values of a_{accept_min} and a_{accept_max} are determined from $a_{raw\_optimal}$ according to the equation (62). We can get acceptable optimal values once the system error is minimal.

$$\left\{\begin{array}{l} for \begin{cases} a_{1\_accept} = a_{1\_accept\_min} : i : a_{1\_accept\_max} \\ a_{2\_accept} = a_{2\_accept\_min} : j : a_{2\_accept\_max} \end{cases} \\ if \;\; e(t) = e(t)_{min} \\ \quad \begin{cases} a_{1\_accept\_optimal} = a_{1\_accept} \\ a_{2\_accept\_optimal} = a_{2\_accept} \end{cases} \\ else \begin{cases} a_{1\_accept\_optimal} = a_{1\_accept+i} \\ a_{2\_accept\_optimal} = a_{2\_accept+j} \end{cases} \end{array}\right\} \tag{61}$$

$$\begin{aligned} a_{1\_accept\_min} &= a_{1\_raw\_optimal} - a_{1\_limit} \\ a_{1\_accept\_max} &= a_{1\_raw\_optimal} + a_{1\_limit} \\ a_{2\_accept\_min} &= a_{2\_raw\_optimal} - a_{2\_limit} \\ a_{2\_accept\_max} &= a_{2\_raw\_optimal} + a_{2\_limit} \end{aligned} \tag{62}$$

C. ASSISTED TORQUE MODEL

The diagram of the EPS control system is shown in Figure 2. This system has two components: an ideal module and a control module. The ideal module is used to calculate the ideal output value ($\theta_{m\_ref\_}$). The ideal module includes a model of ideal electric power steering and a model of the assisted torque map. The inputs to the ideal electric power steering model are driver torque (T_d) and ideal assisted torque (T_{a_ideal}). The driver generates driver torque, while ideal assisted torque is looked up from the assisted torque map (Figure 3). The input to the assisted torque map is driver torque and motion velocity. The assisted torque curve map is built based on linear lines with relative accuracy.

$$u(t) = -L_m \left(\begin{array}{l} K_2 \dfrac{K_c}{J_{eq} i} x_1 + K_2 \left(c_1 \dfrac{B_{eq}}{J_{eq}} - \dfrac{K_c + K_r r_p^2}{J_{eq} i^2} + 1 - c_1^2 \right) x_3 - \dfrac{K_t}{L_m} x_4 + K_2 \dfrac{K_t}{J_{eq}} x_5 \\ + K_2 \left(- \left(\dfrac{c_1 B_{eq} + J_{eq}\left(1 + c_1^2\right)}{J_{eq}} + \dfrac{K_1 R_m}{K_2 L_m} \right) x_{ref} - \left(\dfrac{B_{eq}}{J_{eq}} + \dfrac{K_1}{K_2} \right) \dot{x}_{ref} - \ddot{x}_{ref} \right) - K_2 \dfrac{T_r}{J_{eq} i} \end{array} \right) \tag{56}$$

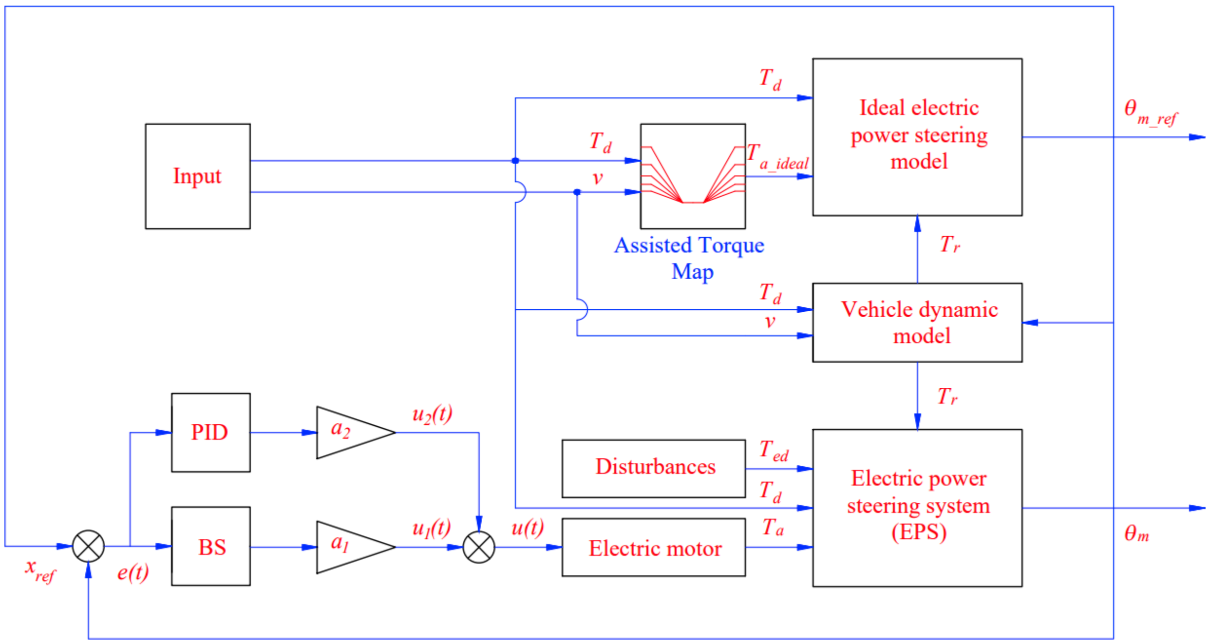

FIGURE 2. **Control system scheme.**

The ideal module's output is the control module's input ($\theta_{m\_ref\_} = x_{ref}$). The control module includes an integrated controller designed in this article and an EPS model (including an electric motor). The input to the EPS model includes driver torque, assisted torque, and other external disturbances. Assisted torque is obtained from the electric motor, which is controlled by the controller based on the voltage signal $u(t)$.

For both modules, the vehicle dynamics model calculates the road reaction torque value (T_r), described through the equations above. Inputs to the vehicle dynamics model are driver torque, velocity, and steering motor angle.

According to [70], assisted torque is determined by the following equation:

$$T_{a\_ideal} = \begin{cases} 0 & 0 \le T_d < T_{d0} \\ f\left(v, T_d\right) & T_{d0} \le T_d < T_{dmax} \\ T_{a\_max} & T_d \ge T_{dmax} \end{cases} \tag{63}$$

where: $f(v, T_d)$ is a defined function of assisted torque. In fact, $f(v, T_d)$ is a nonlinear function that depends on the velocity and driver torque. To simplify the problem, we can use an approximate linear function instead of a complex nonlinear function. The assisted torque function is represented by equation (64).

$$f\left(v, T_d\right) = \left(b_1 v^2 + b_2 v + b_3\right)\left(T_d - T_{d0}\right) \tag{64}$$

With: b_i are experimental coefficients.

Figure 3 illustrates the value of assisted torque according to driver torque at different speed values. According to the results in Figure 3, the electric motor will not operate when $T_d < T_{d0}$. The value of T_{a_ideal} increases gradually and is proportional to T_d until it reaches its maximum value

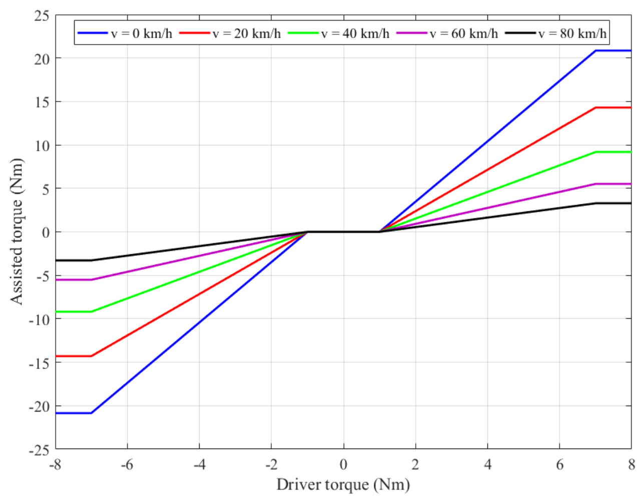

FIGURE 3. **Assisted torque map.**

($T_{a\_ideal} = T_{a\_max}$, corresponding to T_{dmax}). Then, this value will remain stable even when $T_d > T_{dmax}$. When the vehicle steers at $v = 0$ km/h, the value of assisted torque is the largest. This value gradually decreases as the vehicle's speed increases.

III. SIMULATION AND RESULT

A. SIMULATION CONDITIONS

The simulation process evaluates the control system's quality established in this article. This process occurs in the MATLAB-Simulink environment. The input to the simulation problem is the change in driver torque, and the output is the

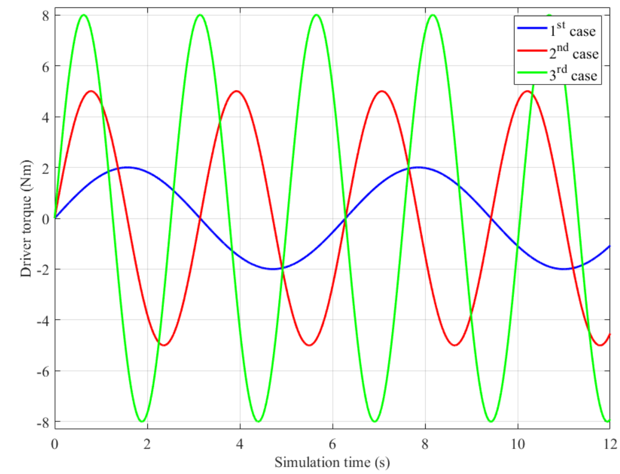

FIGURE 4. Driver torque (T_d).

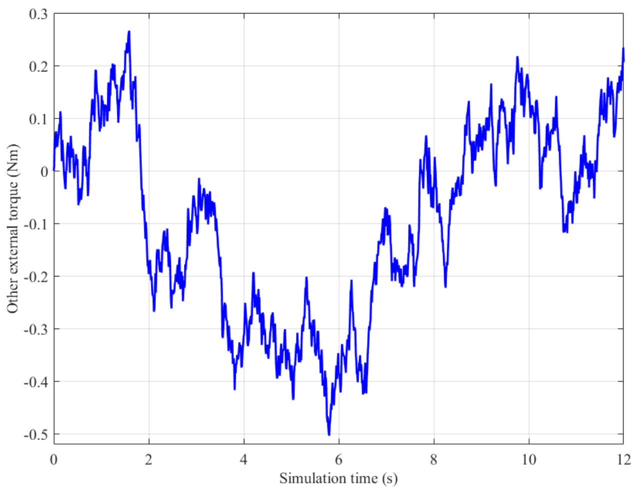

FIGURE 5. Other external torque.

values of the EPS system model, including steering column angle, steering column rate, steering motor angle, steering motor rate, motor current, and assisted torque. Three cases are investigated, corresponding to three values of driver torque (Figure 4). We use sine signals of different amplitudes and frequencies.

There are three data types shown in each investigated plot.

+ The first scenario: the steering system is controlled by the integrated algorithm designed in this article (BSPID). Road surface conditions and other influences are collectively referred to as other external disturbances. These are referred to as T_{ed}, which is illustrated in Figure 5. This is a type of random excitation, and it is determined by (65). Their value (T_{ed}) is integrated with the road reaction torque (T_r) in equation (66).

+ The second scenario: the EPS system is controlled by just a simple PID controller.

+ The third scenario: the electric motor is broken, and the steering system operates without support from the electric motor (None). This scenario is equivalent to a car using a mechanical steering system without power assistance.

+ The fourth scenario: a reference signal calculated by an ideal model (Reference). This scenario does not consider the influence of road disturbances and other external factors.

TABLE 1. EPS specifications.

Symbol	Value	Unit	Symbol	Value	Unit
J_c	0.04	kgm²	l_l	1.0	m
B_c	0.072	Nms/rad	l_2	1.8	m
K_c	115	Nm/rad	J_z	4240	kgm²
L_m	0.0056	H	$C_{\alpha 1}$	46800	N/rad
R_m	0.37	Ω	$C_{\alpha 2}$	46800	N/rad
K_t	0.05	Nm/A	l_c	0.033	m
i	13.65	-	M	1814	kg
J_m	0.0004	kgm²	K_r	43000	N/mrad
B_m	0.0032	Nms/rad	B_r	3820	Ns/m
M_r	32	kg	l_n	0.33	m
r_p	0.007	m			

$$T_{ed}(t) = -2\pi \int_0^t \left[f T_{ed}(\tau) - \sqrt{G v}\,\omega(\tau) \right] d\tau \tag{65}$$

$$T_r = l_c r_p \frac{\cos^2(\gamma_k)\cos^2(\gamma_c)}{l_n} F_{y1} + T_{ed} \tag{66}$$

Equation (66) is used for the first scenario (BSPID), second scenario (PID), and third scenario (None), while the final scenario (Reference) only uses equation (20).

The values of the EPS system parameters are listed in Table 1.

B. RESULT AND DISCUSSION

1) THE FIRST CASE

v_1 = 20 km/h: In the first case, the driver torque is relatively small. Its amplitude and frequency are 2 Nm and 1 rad/s, respectively (Figure 4). Figure 6 illustrates the dynamic parameters change over time when the vehicle steers at a speed of $v_1 = 20$ km/h. The first subplot in Figure 6 shows the change in the steering column angle throughout the simulation period (12 s). According to this result, the value of the steering column angle changes periodically according to a sine function, similar to driver torque. The value of BSPID closely follows the reference signal. The maximum reference value is 1.49 rad, while the peak value for the BSPID scenario is 1.51 rad. There is an error in the results of the second scenario (PID). These results are smaller than the ideal value (1.40 rad). Besides, phase differences also appear in this scenario. If the EPS system is broken, the steering column angle will decrease even though the driver torque remains unchanged. The maximum value of the steering column angle in this scenario is only 0.71 rad, about 47.02% compared to the BSPID scenario. Simply put, the steering column angle and steering angle will decrease once the electric motor is not running. In this article, we use the RMS (root mean square)

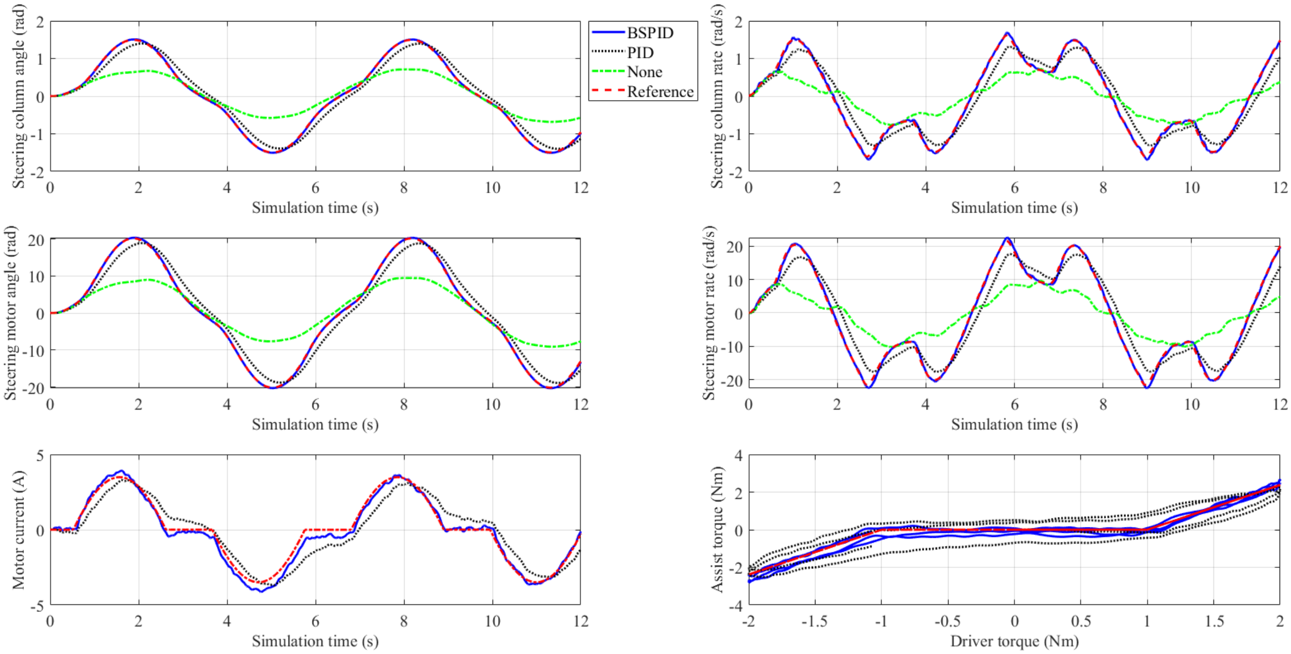

FIGURE 6. Simulation result (1st case - v_1).

criterion to evaluate the changes in output parameters over a continuous period. The calculation results show that the RMS value of the steering column angle reaches 0.92 rad, 0.86 rad, 0.46 rad, and 0.91 rad, respectively, corresponding to four scenarios: BSPID, PID, None, and Reference. The difference between the BSPID and Reference signals is negligible, while these results are twice as significant as those for the None signal.

The second subplot in Figure 6 shows that the steering column rate obtained from the BSPID controller always follows the desired signal. According to research findings, their maximum error is 0.08 rad/s, while the RMS error is only 0.01 rad/s. The difference between these two signals is tiny. The errors of the PID scenario are 0.30 rad/s and 0.09 rad/s, respectively, compared to the standard. However, when the EPS system is broken, the maximum steering column rate only reaches 0.77 rad/s (None). This reduces their RMS value to only 0.45 rad/s. Because other disturbances affect the steering system, the (None) signal's changing trajectory is unpredictable. However, we can easily predict the trajectory of the BSPID scenario, even though it is still subject to other disturbances.

The change in steering motor angle and steering motor rate is similar to the change in steering column angle and steering column rate. However, their value is much greater. According to simulation results, the maximum value of the steering motor angle is 9.45 rad if the steering system is broken. In the regular operation of the EPS system, this value reaches 20.35 rad (BSPID), 0.20 rad higher than the ideal condition, or 18.89 rad (PID), 1.26 rad lower than the reference result. Their RMS values are 12.34 rad, 11.57 rad, 6.09 rad, and 12.25 rad, in the order BSPID, PID, None, and Reference. The difference between BSPID and Reference signals is negligible for steering motor rate, only about 4.59% for the maximum value and 0.98% for the average value. Compared to the scenarios mentioned above, the value of the None scenario is only about half. One thing that should be noted is that the steering motor angle and steering motor rate values persist even when the electric motor is not running. This occurs due to the driver's action through driver torque, i.e., T_d rotating the electric motor instead of using i_m current; see equations (6) and (7).

According to Figure 6, the actual current tends to track the ideal current. Deviations occur at some point, corresponding to changes in other disturbances (Figure 5). In general, the current value in this condition is small, reaching only 4.12 A for the maximum value and 2.09 A for the RMS value (BSPID). For the PID scenario, these figures are 3.69 A and 1.91 A, respectively. The final subplot describes the relationship between driver torque (T_d) and assisted torque (T_a). This result shows that the actual power steering characteristic is a curve that closely follows the desired signal with minor errors.

$v_2 = 40$ *km/h:* As the moving speed increases, the resistance from the road surface also increases. According to Figure 3, assisted torque tends to decrease as speed increases. A reasonable prediction is that the output values of the simulation problem will decrease as the velocity increases.

According to Figure 7, the steering column angle increases from zero to the peak value (1.05 rad) when the steering system is controlled by the BSPID algorithm. This increase always closely tracks the desired signal (Reference). The

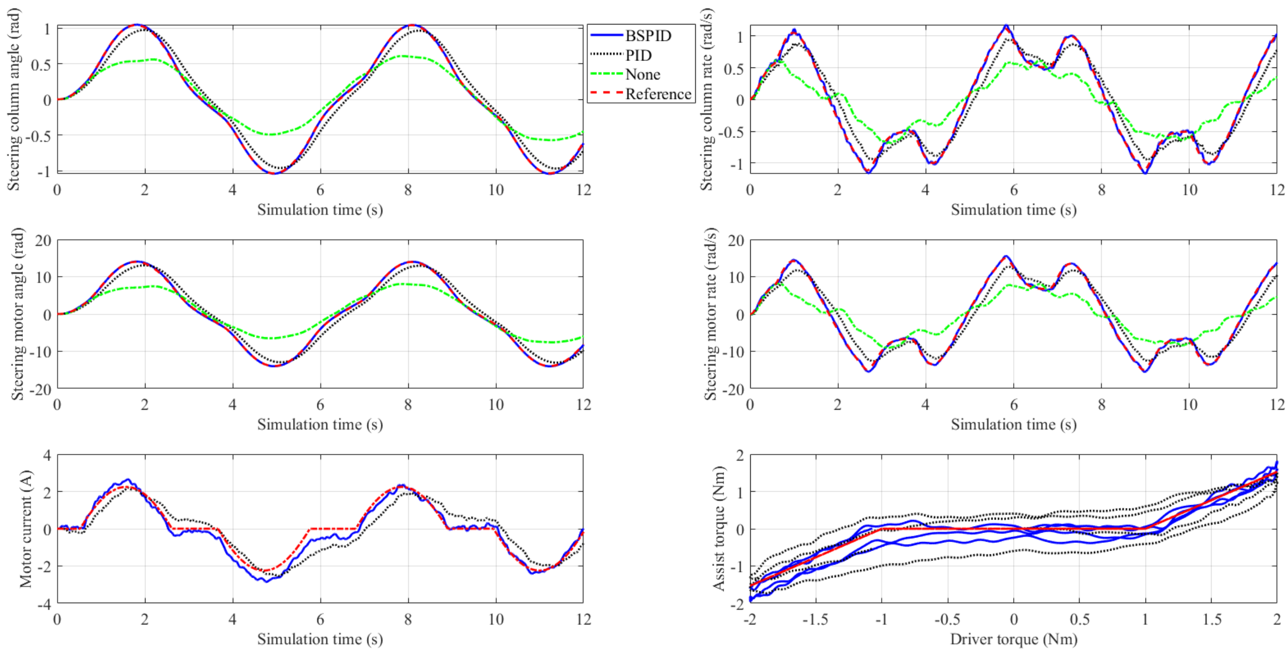

FIGURE 7. **Simulation result (1st case - v_2).**

difference between them is negligible, only about 0.01 rad. According to the RMS criterion, the difference between the BSPID and Reference signals is approximately zero (results have been rounded). These values are 0.97 rad and 0.61 rad, respectively, when a traditional PID controller controls the system. However, the steering column angle only reaches 0.61 rad for the maximum value and 0.39 rad for the RMS value if the electric motor cannot operate. The variation of the steering column rate is similar to the steering column angle, with the difference between the controlled signal and the reference signal being very small (see Table 2). In general, both steering column angle and steering column rate decrease as speed increases.

The steering motor angle and steering motor rate change in condition v_2 is similar to condition v_1. However, their value decreased slightly. According to the results in Figure 8, the value of BSPID always follows the desired signal even when the system is subjected to external disturbances.

The control current decreases in the condition $v_2 = 40$ km/h, compared to v_1 (Figure 7). The error between the set and actual signals is most significant when other external factors are largest (Figure 5). The maximum value of control current is 2.85 A, a decrease of 1.27 A compared to condition v_1 (BSPID). Its RMS value is also 1.39 A, only 66.51% of the previous condition. The difference between Reference and BSPID signals is insignificant. The characteristic curve of assisted torque is nonlinear. Its changes are irregular. This is caused by the impact of external disturbances.

$v_3 = 60$ *km/h:* Once the vehicle speed increases, the control current will decrease sharply, meaning the assisted torque will decrease sharply (Figure 3). According to the results in Figure 8, the maximum value of the current is only 1.95 A when applying the BSPID algorithm to the steering system, while its RMS value is 0.91 A. The decrease in the value of the current means that booster performance is reduced. The figures for the PID scenario are 1.75 A and 0.83 A, respectively, lower than the BSPID scenario.

For the remaining outputs of the electric power steering system model, the signal received from BSPID always closely follows the desired signal. Looking at subplots closer, we can see that the gap between the BSPID and None signals tends to decrease as the assisted performance degrades. Once the velocity increases, the difference between these results is negligible. The error of the results obtained from the PID scenario is much larger than the BSPID scenario. The results of this condition should be referred to in Table 2.

2) THE SECOND CASE

The first case uses an input signal with a small amplitude and frequency. Therefore, the performance of the EPS system cannot be fully exploited. In the second case, we propose to use a steering signal with a higher frequency and amplitude (2 rad/s and 5 Nm). Similar to the previous case, the change of output parameters is investigated in three situations: $v_1 = 20$ km/h, $v_2 = 40$ km/h, and $v_3 = 60$ km/h.

$v_1 = 20$ *km/h:* As driver torque increases, the output values of the steering model also increase. The steering column angle's peak value can be up to 4.82 rad when steering at speed $v_1 = 20$ km/h (Figure 9). This value is obtained when applying the BSPID algorithm to control the steering system. Its RMS value is 2.96 rad, approximately the RMS value of

TABLE 2. Simulation result (1st case).

	Steering column angle (rad)		Steering column rate (rad/s)		Steering motor angle (rad)		Steering motor rate (rad/s)		Motor current (A)	
$v_1 = 20$ km/h										
	Max	RMS	Max	RMS	Max	RMS	Max	RMS	Max	RMS
BSPID	1.51	0.92	1.69	0.99	20.35	12.34	22.55	13.40	4.12	2.09
PID	1.40	0.86	1.31	0.89	18.89	11.57	17.70	12.08	3.69	1.91
None	0.71	0.46	0.77	0.45	9.45	6.09	10.20	6.02		
Reference	1.49	0.91	1.61	0.98	20.15	12.25	21.56	13.27	3.49	1.97
$v_2 = 40$ km/h										
BSPID	1.05	0.64	1.18	0.71	14.05	8.61	15.58	9.49	2.85	1.39
PID	0.97	0.61	0.96	0.63	13.06	8.13	12.70	8.41	2.54	1.26
None	0.61	0.39	0.69	0.39	8.04	5.15	9.10	5.22		
Reference	1.04	0.64	1.12	0.70	13.97	8.57	14.93	9.42	2.24	1.28
$v_3 = 60$ km/h										
BSPID	0.77	0.49	0.84	0.51	10.23	6.49	11.03	6.84	1.95	0.91
PID	0.72	0.47	0.72	0.46	9.60	6.27	9.45	6.16	1.75	0.83
None	0.54	0.35	0.64	0.35	7.07	4.58	8.33	4.59		
Reference	0.76	0.49	0.79	0.51	10.20	6.46	10.52	6.80	1.35	0.79

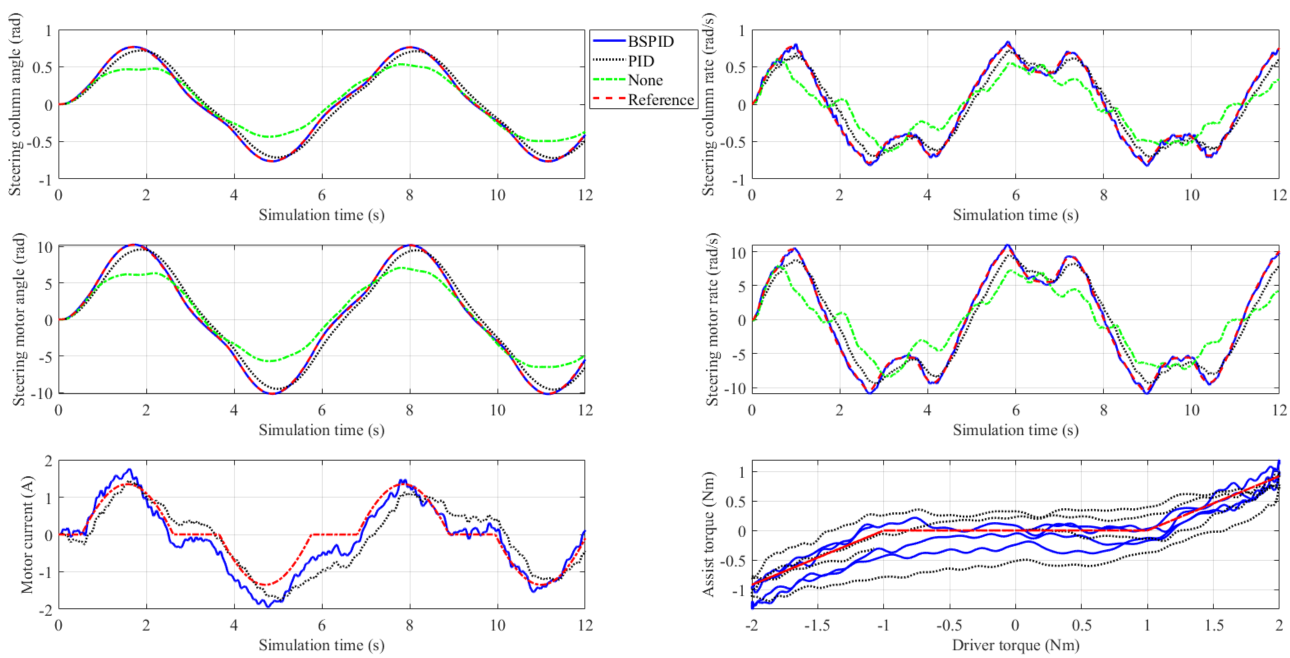

FIGURE 8. Simulation result (1st case - v_3).

the reference signal (2.91 rad). The change in the BSPID signal always follows the reference signal. Regarding the PID controller, these values are 4.01 rad and 2.48 rad, respectively. Compared to the BSPID scenario, the errors between these results are much more significant. The phase derivation phenomenon also occurs strongly when the vehicle moves at low speed (PID). This can cause some adverse effects on steering. The steering column angle only reaches 1.78 rad and 1.06 rad (peak value and RMS value) if the electric motor cannot operate. To put it more simply, the steering wheel and steering angles will decrease once the EPS system has a problem. Regarding steering column rate, data from the two scenarios (BSPID and Reference) always follow each other with insignificant errors. However, the value belonging to the None scenario is much lower than the other two scenarios. Besides, the changes in the steering motor angle and steering motor rate tend to be similar to the steering column angle and steering column rate. However, their amplitude is more

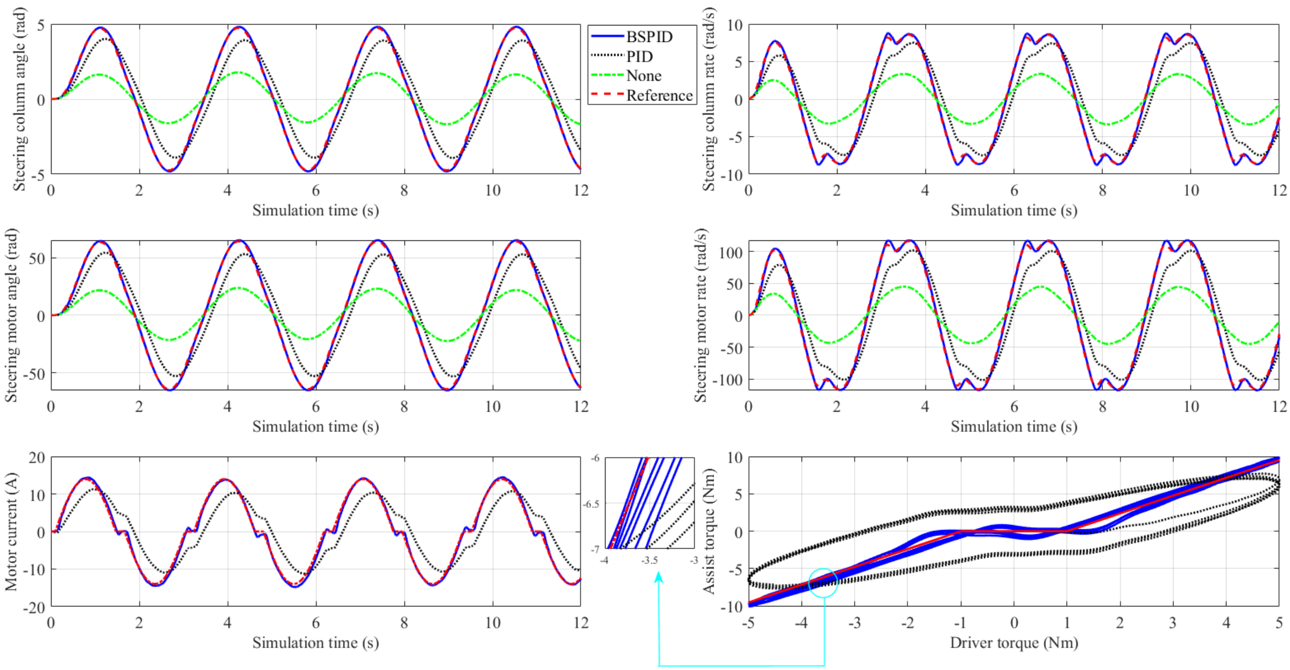

FIGURE 9. Simulation result (2^{nd} case - v_1).

TABLE 3. Simulation result (2^{nd} case).

	Steering column angle (rad)		Steering column rate (rad/s)		Steering motor angle (rad)		Steering motor rate (rad/s)		Motor current (A)	
v_1 = 20 km/h										
	Max	RMS	Max	RMS	Max	RMS	Max	RMS	Max	RMS
BSPID	4.82	2.96	8.81	6.64	65.15	40.04	117.75	89.83	14.78	8.71
PID	4.01	2.48	7.51	5.35	54.27	33.54	101.56	72.43	11.28	6.66
None	1.78	1.06	3.38	2.37	23.76	14.17	45.06	31.62		
Reference	4.74	2.91	8.58	6.53	64.09	39.42	116.20	88.29	13.96	8.52
v_2 = 40 km/h										
BSPID	3.39	2.09	6.72	4.72	45.68	28.10	89.25	63.57	9.64	5.67
PID	2.83	1.75	5.24	3.92	38.08	23.61	70.33	52.82	7.34	4.20
None	1.63	0.97	3.15	2.19	21.75	12.92	41.65	29.18		
Reference	3.35	2.07	6.31	4.66	45.19	27.81	84.77	62.78	8.97	5.56
v_3 = 60 km/h										
BSPID	2.49	1.55	5.33	3.54	33.36	20.76	70.61	47.37	6.01	3.40
PID	2.14	1.36	4.05	2.96	28.73	18.14	54.05	39.67	4.78	2.67
None	1.53	0.91	3.00	2.07	20.31	12.09	39.73	27.40		
Reference	2.47	1.53	5.04	3.49	33.10	20.55	67.38	46.71	5.39	3.29

extensive. The simulation results should be referred to in Table 3.

In this condition, the current used for the motor is quite large. Simulation results show that the maximum current is 14.78 A (BSPID), 0.82 A higher than the desired threshold. The RMS values of BSPID, PID and Reference are 8.71 A, 6.66 A, and 8.52 A, respectively. Overall, the difference between BSPID and Reference is inconsiderable. The last subplot in Figure 9 shows the dependence between assisted and driver torque. The characteristic curve changes continuously and follows the desired signal once the system is controlled by the BSPID algorithm. On the contrary, the deviation between the output value obtained from the PID controller and the desired value is quite significant.

$v_2 = 40$ *km/h:* Figure 10 shows the results when the car steers at a speed of $v_2 = 40$ km/h. Compared to condition v_1, the output values decrease as the velocity increases. The simulation results show that the peak value of the steering

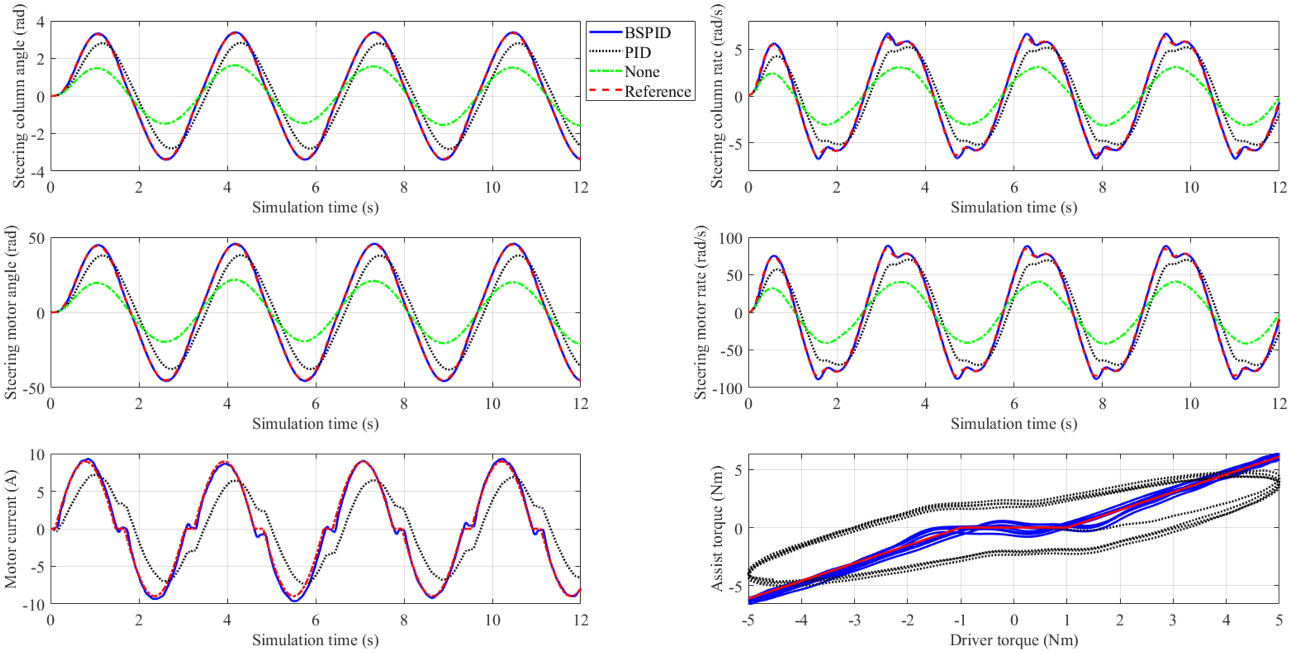

FIGURE 10. Simulation result (2nd case - v_2).

column angle is 3.39 rad. This value is achieved when using the BSPID controller for the steering system. Compared to the desired threshold, this value is only 0.04 rad higher. In addition, the difference in RMS value between the two scenarios (BSPID and Reference) does not exceed 0.02 rad. The difference between the value obtained from the PID scenario and the desired value is 0.52 rad (maximum value) and 0.32 rad (RMS value), much higher than the BSPID scenario. The value of the steering column angle drops by more than half (1.63 rad and 0.97 rad) once the EPS system has a problem (None). Regarding the steering column rate, the output signal obtained from BSPID continuously tracks the Reference with insignificant errors of 6.50% (maximum) and 1.29% (RMS). However, the values obtained from the (PID) and (None) scenarios are much lower than the scenario mentioned above.

Regarding the steering motor angle, their changing trend is not much different from that of the steering column angle. The same is true for steering motor rate (see Figure 10). The difference between the controlled signal and the desired signal is minimal (BSPID), while the error between the uncontrolled signal and the reference signal is considerable. The simulation results are listed in Table 3.

According to Figure 10, the motor current decreases as speed increases from v_1 to v_2. According to these results, the peak current value decreases from 14.78 A to 9.64 A (BSPID) and from 11.28 A to 7.34 A (PID), while the RMS value changes from 8.71 A to 5.67 A (BSPID) and from 6.66 A to 4.20 A (PID). The results obtained from the BSPID scenario are closer to the ideal value than the PID scenario.

$v_3 = 60$ *km/h:* In the following condition, the car's moving speed is raised higher, $v_3 = 60$ km/h. The control current needs to be reduced to ensure the car's stability when driving. As a result, the assisted torque must also decrease (Figure 3). Therefore, the steering column angle and steering column rate also decrease. According to Figure 11, the peak value of the steering column angle is reduced to 2.49 rad when the BSPID algorithm controls the EPS system. This value is approximately the desired value (2.47 rad), while the result obtained from the PID algorithm is only 2.14 rad. However, the maximum steering column angle is only 1.53 rad when the electric power steering system is damaged. Their RMS values are 1.55 rad, 1.36 rad, 0.91 rad, and 1.53 rad in the order BSPID, PID, None, and Reference. The difference between the results is insignificant for the steering column rate.

Power consumption in this condition is reduced compared to the previous two conditions. The motor's maximum current is only about 6 A, while its RMS current is 3.40 A (BSPID). The simulation results in the second case are listed in Table 3.

3) THE THIRD CASE

Driver torque in the first and second cases is both smaller than T_{dmax}. Therefore, it is necessary to use a more considerable T_d value (exceeding the limitation of T_{dmax}) to investigate the system's stability. This is done in the third case. According to Figure 4, the driver torque, in this case, has an amplitude of 8 Nm and a frequency of 2.5 rad/s.

$v_1 = 20$ *km/h:* The change in dynamic parameters of the steering system is most significant when the car steers in condition v_1. The results in Figure 12 show that the output value obtained from BSPID always closely follows the reference signal. If the value of T_d increases, the steering column angle also increases. According to the results in Figure 12, the steering column angle can be up to 7.53 rad when applying

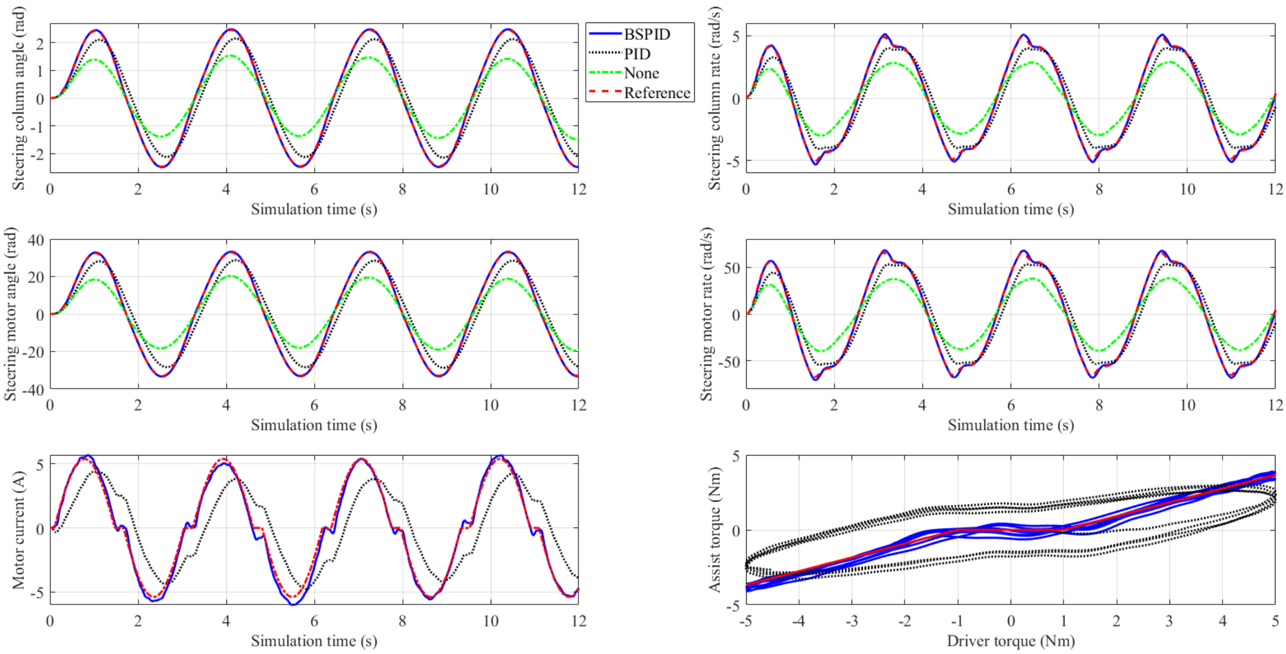

FIGURE 11. Simulation result (2nd case - v_3).

the BSPID algorithm to the steering system, 0.13 rad higher than the reference value. Additionally, their RMS values reach 5.09 rad and 4.99 rad, respectively. The values of the PID scenario are lower and reach 6.06 rad and 3.96 rad, respectively. Steering performance will be impaired once the electric motor is damaged. The value of the steering column angle drops sharply to 2.72 rad (the maximum value) and 1.75 rad (the RMS value) for the None scenario. Concerning steering column rate, their changes become stronger as driver torque increases. In this condition, the electric motor operates more powerfully, leading to a sharp increase in steering motor angle and steering motor rate values. Although influenced by other external factors, the signal received from BSPID still follows the reference signal with high accuracy. However, the error between the results is quite significant if we only use the single PID controller instead of the BSPID nonlinear integrated controller.

Under this condition, the motor current can reach up to 22.87 A (BSPID), which is 9.22% higher than the expected value considering their maximum value. However, the difference between the RMS values is only 3.05% (15.55 A and 15.09 A). The dependence between driver torque and assisted torque is depicted in the last subplot in Figure 12. According to this result, the value of assisted torque is almost unchanged when the driver torque exceeds the allowable limit (T_{dmax}). This helps demonstrate the controller's effectiveness established in this article.

$v_2 = 40$ km/h: At speed $v_2 = 40$ km/h, the control current decreases. According to the results in Figure 13, the maximum current when applying the BSPID algorithm is 14.77 A, down 8.10 A compared to condition v_1. In addition, its RMS value also decreases sharply, from 15.55 A to 9.95 A. The actual current signal always follows the reference signal. Regarding the PID controller, the difference between the obtained results and the desired value is significant. For remaining outputs (steering column angle, steering column rate, steering motor angle, and steering motor rate), the output (obtained from the BSPID controller) always follows the desired signal with negligible error, even though the system is affected by other external factors. Once the driver torque exceeds its limit value ($T_d| > T_{dmax}$), the steering torque will be maintained at the maximum level and will not increase.

$v_3 = 60$ km/h: Like the abovementioned conditions, the model output values will decrease once the velocity increases. This is indicated by subplots in Figure 14. Overall, there are no significant differences in the change trend between conditions. The simulation results in the third case are listed in Table 4.

This research shows that the motor current is smaller, meaning it is more energy efficient, compared to using a single controller optimized by the ACO algorithm [17]. In addition, when controlled by the BSPID algorithm, the system response is more efficient than that of PID and H_2 [28]. Finally, the chattering phenomenon does not occur when we apply the BSPID technique to the EPS system, while other control algorithms still cause this phenomenon [27], [30], [32], [36].

Based on the simulation results, some statements are made as follows:

+ If the value of $T_d < T_{d0}$, the electric motor does not work. If the value of $T_d > T_{dmax}$, assisted torque (T_a) will

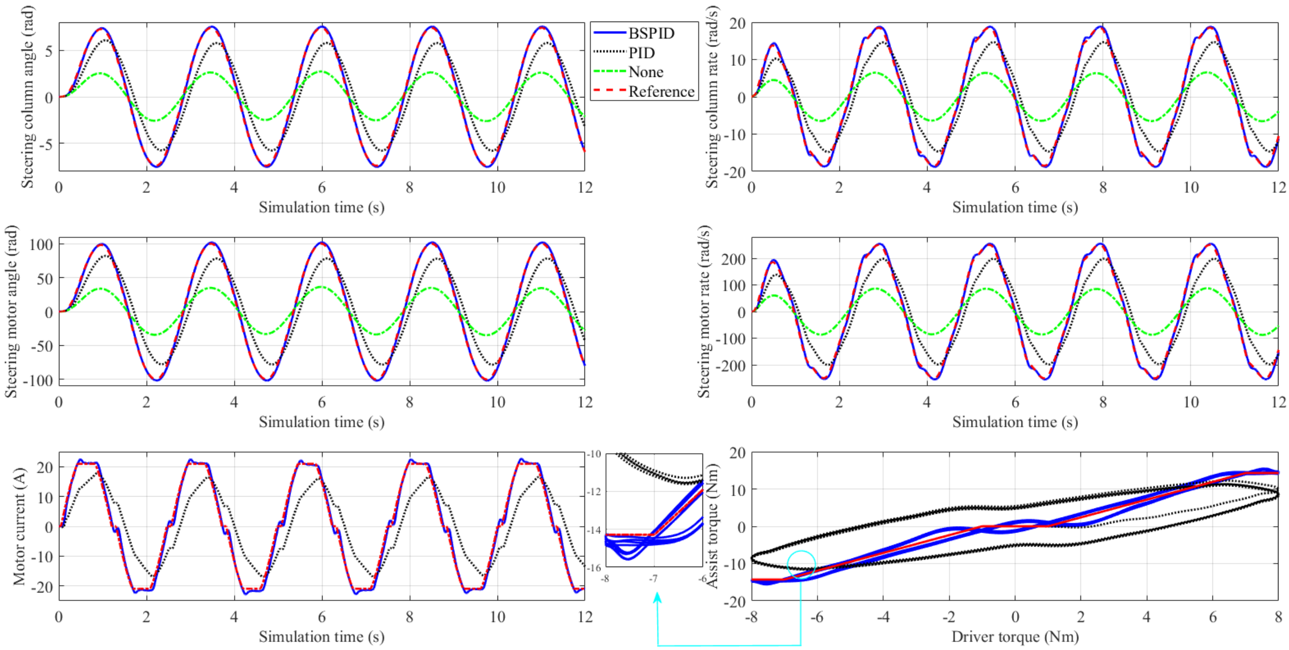

FIGURE 12. Simulation result (3rd case - v_1).

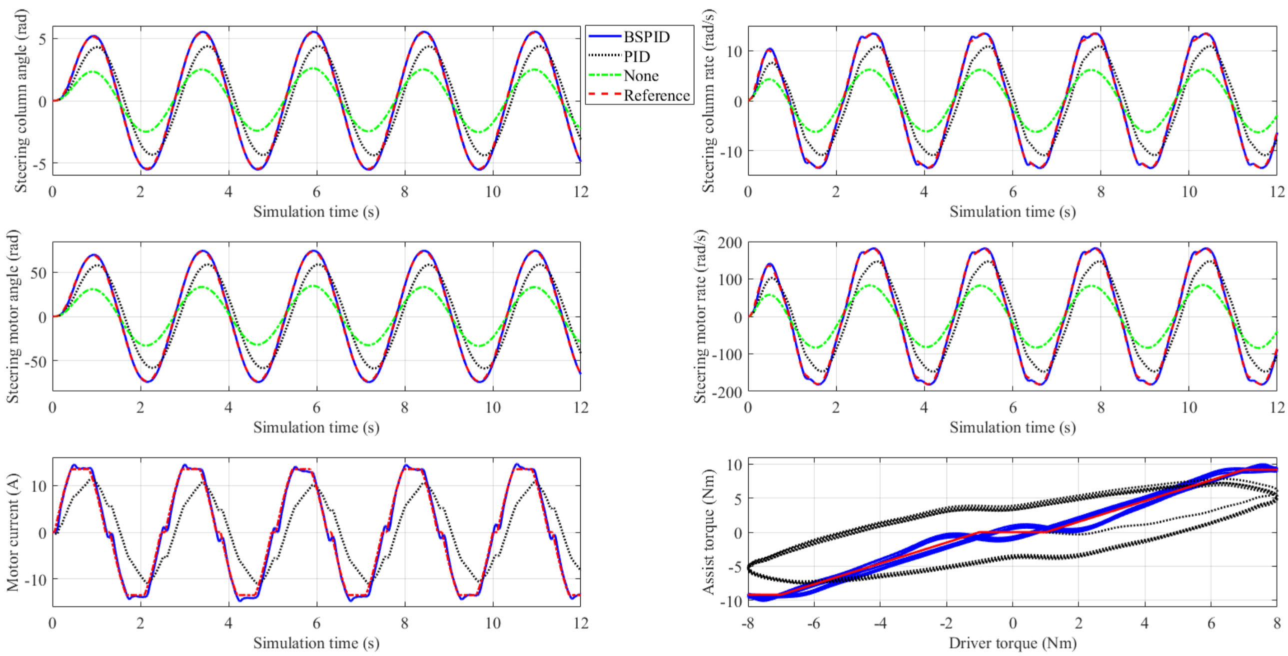

FIGURE 13. Simulation result (3rd case - v_2).

maintain its limit state. The value of assisted torque increases when the speed decreases, and vice versa.

+ If driver torque does not change, the output values (steering column angle, steering column rate, steering motor angle, steering motor rate, and motor current) will decrease as the speed increases. The cause is decreased assisted torque, which is inversely proportional to speed (as in the above statement). This helps maintain the car's stability when steering and avoids rollover instability in some dangerous conditions.

+ If the velocity does not change, the output values will increase as the driver torque increases. This is entirely consistent with reality. This will make steering easier if we want to steer strongly or suddenly change direction. However, the vehicle's speed will have a limit on this assistance.

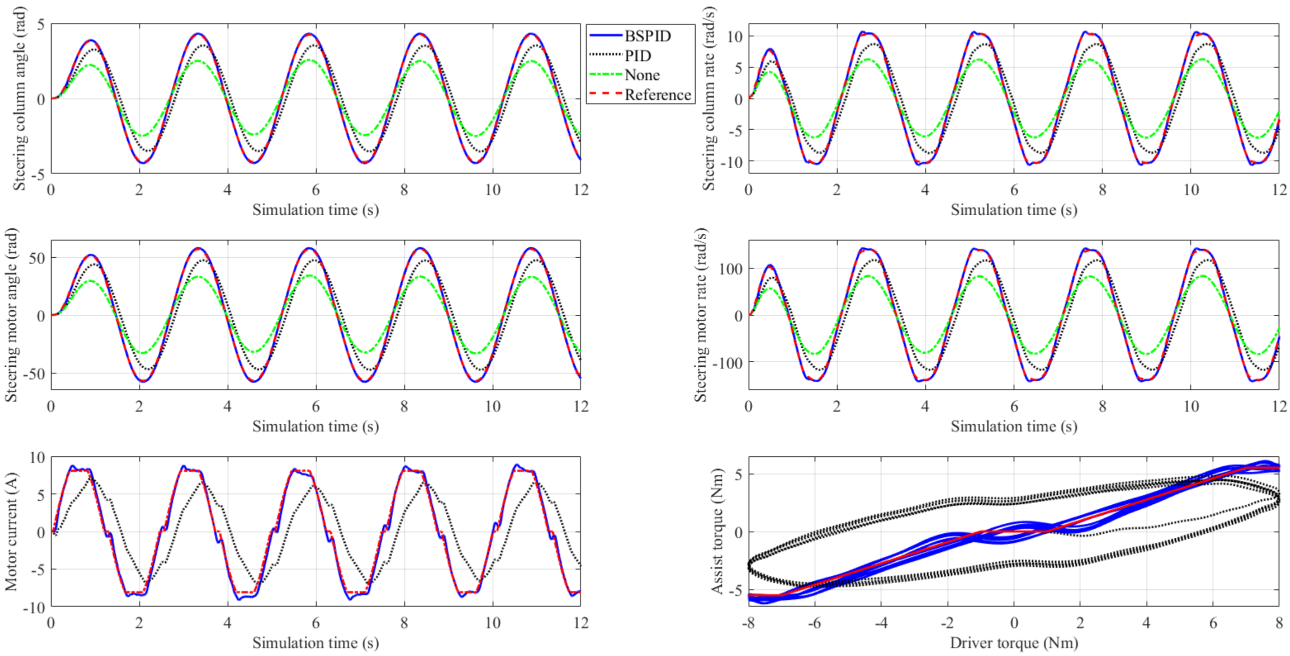

FIGURE 14. Simulation result (3rd case - v_3).

TABLE 4. Simulation result (3rd case).

	Steering column angle (rad)		Steering column rate (rad/s)		Steering motor angle (rad)		Steering motor rate (rad/s)		Motor current (A)	
	v_1 = 20 km/h									
	Max	RMS	Max	RMS	Max	RMS	Max	RMS	Max	RMS
BSPID	7.53	5.09	18.83	12.94	101.93	67.90	254.75	174.92	22.87	15.55
PID	6.06	3.96	14.82	9.66	82.13	53.67	200.62	130.81	17.89	10.79
None	2.72	1.75	6.57	4.43	36.34	23.43	87.76	59.19		
Reference	7.40	4.99	18.50	12.67	100.12	66.58	250.55	171.36	20.94	15.09
	v_2 = 40 km/h									
BSPID	5.52	3.65	13.50	9.74	74.53	49.25	182.11	130.20	14.77	9.95
PID	4.37	2.93	10.94	7.44	59.04	39.49	147.54	100.35	11.46	6.79
None	2.60	1.65	6.34	4.37	34.66	21.96	84.30	58.17		
Reference	5.46	3.60	13.39	9.58	73.58	48.53	180.75	129.10	13.46	9.71
	v_3 = 60 km/h									
BSPID	4.30	2.87	10.67	7.54	57.78	38.48	142.01	101.12	9.10	6.00
PID	3.53	2.32	8.71	6.11	47.36	31.20	116.86	81.94	7.06	4.23
None	2.56	1.56	6.27	4.31	33.10	20.95	83.43	57.35		
Reference	4.24	2.82	10.38	7.41	56.96	37.92	139.51	99.50	8.08	5.80

+ If the electric power steering motor is broken, the output values will decrease compared to normal operating conditions.

+ In all investigated conditions, the output signal obtained from the BSPID always follows the reference signal, even though the steering system is subject to other external disturbances. Therefore, the system's stability is always guaranteed under many motion conditions.

IV. CONCLUSION

EPS systems have many outstanding advantages compared to conventional mechanical steering systems. In this article, we propose to use the integrated algorithm to control the electric motor of the EPS system to ensure the stability and efficiency of the system. The final control signal is synthesized from two component controllers: the BS controller and the PID controller. The dynamic model of the EPS system is designed with five state variables and considers the influence of road reaction torque and other external disturbances. Compared with previous studies, the combination proposed in this work is entirely new and takes advantage of the outstanding advantages of both backstepping and PID techniques. In addition, we can approximately calculate the change in road reaction torque instead of assuming it to be a known value. This makes the control process more stable and accurate.

According to research findings, the output signals of the steering system model always closely follow the reference signal. In all simulation cases, the errors between them are negligible. System performance and stability are always guaranteed once the BSPID algorithm is applied to control the EPS system. The system's response is timely, and the chattering phenomenon does not occur. The output parameters of the EPS model can be strongly degraded if the electric power steering system loses control. A slight limitation still exists regarding the variation of motor current and assisted torque. This can be solved by combining this algorithm with intelligent control techniques, such as fuzzy systems or neural networks. In the near future, we will conduct some experiments to prove the effectiveness of the algorithm designed in this article.

REFERENCES

[1] L. Xia and H. Jiang, "An electronically controlled hydraulic power steering system for heavy vehicles," *Adv. Mech. Eng.*, vol. 8, no. 11, Nov. 2016, doi: 10.1177/1687814016679566.

[2] J. Hur, "Development of an electric motor-driven pump unit for electro-hydraulic power steering with 42V power-net," *Int. J. Automot. Technol.*, vol. 11, no. 4, pp. 593–600, Aug. 2010, doi: 10.1007/s12239-010-0071-8.

[3] M. B. Baharom, K. Hussain, and A. J. Day, "Design of full electric power steering with enhanced performance over that of hydraulic power-assisted steering," *Proc. Inst. Mech. Eng., D, J. Automobile Eng.*, vol. 227, no. 3, pp. 390–399, Mar. 2013, doi: 10.1177/0954407012468413.

[4] J. Jang, S.-G. Cho, S.-J. Lee, K.-S. Kim, J.-M. Kim, J.-P. Hong, and T. H. Lee, "Reliability-based robust design optimization with kernel density estimation for electric power steering motor considering manufacturing uncertainties," *IEEE Trans. Magn.*, vol. 51, no. 3, pp. 1–4, Mar. 2015, doi: 10.1109/TMAG.2014.2359512.

[5] N. Truemmel, T. Poetzl, and H.-C. Reuss, "Improvements on availability and comfort of electric drives for electric power steering application," in *Proc. 8th IET Int. Conf. Power Electron., Mach. Drives (PEMD)*, Apr. 2016, pp. 1–6, doi: 10.1049/cp.2016.0194.

[6] A. Khalkhali, M. H. Shojaeefard, M. Dahmardeh, and H. Sotoudeh, "Optimal design and applicability of electric power steering system for automotive platform," *J. Central South Univ.*, vol. 26, no. 4, pp. 839–851, Apr. 2019, doi: 10.1007/s11771-019-4053-3.

[7] S. Chung and H. Lee, "Advanced control strategy for electric power steering system to improve steering assist torque stability," in *Proc. 15th Int. Conf. Control, Autom. Syst. (ICCAS)*, Oct. 2015, pp. 1999–2004, doi: 10.1109/iccas.2015.7364696.

[8] Z. Cao and S. Zheng, "MR-SAS and electric power steering variable universe fuzzy PID integrated control," *Neural Comput. Appl.*, vol. 31, no. 4, pp. 1249–1258, Apr. 2019, doi: 10.1007/s00521-017-3157-7.

[9] W. Kim, Y. S. Son, and C. C. Chung, "Torque-overlay-based robust steering wheel angle control of electrical power steering for a lane-keeping system of automated vehicles," *IEEE Trans. Veh. Technol.*, vol. 65, no. 6, pp. 4379–4392, Jun. 2016, doi: 10.1109/TVT.2015.2473115.

[10] B. Arifin, B. Y. Suprapto, S. A. D. Prasetyowati, and Z. Nawawi, "Steering control in electric power steering autonomous vehicle using type-2 fuzzy logic control and PI control," *World Electric Vehicle J.*, vol. 13, no. 3, p. 53, Mar. 2022, doi: 10.3390/wevj13030053.

[11] X. Guan, Y. Zhang, P. Lu, C. Duan, and J. Zhan, "The control strategy of the electric power steering system for steering feel control," *Proc. Inst. Mech. Eng., D, J. Automobile Eng.*, Nov. 2022, doi: 10.1177/09544070221132131.

[12] L. Yaohua, F. Jikang, H. Jie, N. Youfei, and F. Qianlong, "Novel electric power steering control strategies of commercial vehicles considering adhesion coefficient," *Adv. Mech. Eng.*, vol. 12, no. 12, Dec. 2020, Art. no. 168781402098305, doi: 10.1177/1687814020983059.

[13] Y. Li, Z. Yang, D. Zhai, J. He, and J. Fan, "Study on control strategy of electric power steering for commercial vehicle based on multi-map," *World Electric Vehicle J.*, vol. 14, no. 2, p. 33, Jan. 2023, doi: 10.3390/wevj14020033.

[14] X. Guan, Y.-N. Zhang, C.-G. Duan, W.-L. Yong, and P.-P. Lu, "Study on decomposition and calculation method of EPS assist characteristic curve," *Proc. Inst. Mech. Eng., D, J. Automobile Eng.*, vol. 235, no. 8, pp. 2166–2175, Jul. 2021, doi: 10.1177/0954407020987062.

[15] J. Wang, T. Yan, Y. Bai, Z. Luo, X. Li, and B. Yang, "Assistance quality analysis and robust control of electric vehicle with differential drive assisted steering system," *IEEE Access*, vol. 8, pp. 136327–136339, 2020, doi: 10.1109/ACCESS.2020.3010792.

[16] X. Chen, T. Yang, X. Chen, and K. Zhou, "A generic model-based advanced control of electric power-assisted steering systems," *IEEE Trans. Control Syst. Technol.*, vol. 16, no. 6, pp. 1289–1300, Nov. 2008, doi: 10.1109/TCST.2008.921805.

[17] R. Abu Hanifah, S. F. Toha, M. K. Hassan, and S. Ahmad, "Power reduction optimization with swarm based technique in electric power assist steering system," *Energy*, vol. 102, pp. 444–452, May 2016, doi: 10.1016/j.energy.2016.02.050.

[18] R. A. Hanifah, S. F. Toha, S. Ahmad, and Mohd. K. Hassan, "Swarm-intelligence tuned current reduction for power-assisted steering control in electric vehicles," *IEEE Trans. Ind. Electron.*, vol. 65, no. 9, pp. 7202–7210, Sep. 2018, doi: 10.1109/TIE.2017.2784344.

[19] A. Kanungo, M. Mittal, and L. Dewan, "Wavelet based PID controller using GA optimization and scheduling for feedback systems," *J. Interdiscipl. Math.*, vol. 23, no. 1, pp. 145–152, Jan. 2020, doi: 10.1080/09720502.2020.1721708.

[20] T. A. Nguyen, "A new approach to selecting optimal parameters for the sliding mode algorithm on an automotive suspension system," *Complexity*, Jul. 2023, doi: 10.1155/2023/9964547.

[21] D. N. Nguyen and T. A. Nguyen, "Evaluate the stability of the vehicle when using the active suspension system with a hydraulic actuator controlled by the OSMC algorithm," *Sci. Reports*, vol. 12, no. 1, 2022, doi: 10.1038/s41598-022-24069-w.

[22] Z. Zheng and J. Wei, "Research on electric power steering fuzzy PI control strategy based on phase compensation," *Int. J. Dyn. Control*, vol. 11, no. 4, pp. 1867–1879, Aug. 2023, doi: 10.1007/s40435-022-01077-2.

[23] T. A. Nguyen, "A novel approach with a fuzzy sliding mode proportional integral control algorithm tuned by fuzzy method (FSMPIF)," *Sci. Rep.*, vol. 13, no. 1, May 2023, doi: 10.1038/s41598-023-34455-7.

[24] T. A. Nguyen, "Research on the sliding mode—PID control algorithm tuned by fuzzy method for vehicle active suspension," *Forces Mech.*, vol. 11, May 2023, Art. no. 100206, doi: 10.1016/j.finmec.2023.100206.

[25] M. Irmer and H. Henrichfreise, "Design of a robust LQG compensator for an electric power steering," *IFAC-PapersOnLine*, vol. 53, no. 2, pp. 6624–6630, 2020, doi: 10.1016/j.ifacol.2020.12.082.

[26] S. Na, Z. Li, F. Qiu, and C. Zhang, "Torque control of electric power steering systems based on improved active disturbance rejection control," *Math. Problems Eng.*, vol. 2020, pp. 1–13, Apr. 2020, doi: 10.1155/2020/6509607.

[27] D. Lee, K.-S. Kim, and S. Kim, "Controller design of an electric power steering system," *IEEE Trans. Control Syst. Technol.*, vol. 26, no. 2, pp. 748–755, Mar. 2018, doi: 10.1109/TCST.2017.2679062.

[28] W.-Z. Zhao, Y.-J. Li, C.-Y. Wang, T. Zhao, and X.-Y. Gu, "H_∞ control of novel active steering integrated with electric power steering function," *J. Central South Univ.*, vol. 20, no. 8, pp. 2151–2157, Aug. 2013, doi: 10.1007/s11771-013-1719-0.

[29] W. Zhao, Y. Lin, J. Wei, and G. Shi, "Control strategy of a novel electric power steering system integrated with active front steering function," *Sci. China Technol. Sci.*, vol. 54, no. 6, pp. 1515–1520, Jun. 2011, doi: 10.1007/s11431-011-4393-1.

[30] C. Dannöhl, S. Müller, and H. Ulbrich, "H_∞-control of a rack-assisted electric power steering system," *Vehicle Syst. Dyn.*, vol. 50, no. 4, pp. 527–544, Apr. 2012, doi: 10.1080/00423114.2011.603051.

[31] M. Nasri, D. Saifia, M. Chadli, and S. Labiod, "H_∞ static output feedback control for electrical power steering subject to actuator saturation via fuzzy Lyapunov functions," *Trans. Inst. Meas. Control*, vol. 41, no. 12, pp. 3340–3351, Aug. 2019, doi: 10.1177/0142331218824385.

[32] D. Lee, K. Yi, S. Chang, B. Lee, and B. Jang, "Robust steering-assist torque control of electric-power-assisted-steering systems for target steering wheel torque tracking," *Mechatronics*, vol. 49, pp. 157–167, Feb. 2018, doi: 10.1016/j.mechatronics.2017.12.007.

[33] D. N. Nguyen and T. A. Nguyen, "Proposing an original control algorithm for the active suspension system to improve vehicle vibration: Adaptive fuzzy sliding mode proportional-integral-derivative tuned by the fuzzy (AFSPIDF)," *Heliyon*, vol. 9, no. 3, Mar. 2023, Art. no. e14210, doi: 10.1016/j.heliyon.2023.e14210.

[34] T. A. Nguyen, "Design a new control algorithm AFSP (adaptive fuzzy—Sliding mode—Proportional—Integral) for automotive suspension system," *Adv. Mech. Eng.*, vol. 15, no. 2, Feb. 2023, doi: 10.1177/16878132231154189.

[35] T. A. Nguyen, "Advance the efficiency of an active suspension system by the sliding mode control algorithm with five state variables," *IEEE Access*, vol. 9, pp. 164368–164378, 2021, doi: 10.1109/ACCESS.2021.3134990.

[36] G. Kim, S. You, S. Lee, D. Shin, and W. Kim, "Robust nonlinear torque control using steering wheel torque model for electric power steering system," *IEEE Trans. Veh. Technol.*, vol. 72, no. 7, pp. 9555–9560, Jul. 2023, doi: 10.1109/TVT.2023.3248301.

[37] M. A. Sepestanaki, M. H. Barhaghtalab, S. Mobayen, A. Jalilvand, A. Fekih, and P. Skruch, "Chattering-free terminal sliding mode control based on adaptive barrier function for chaotic systems with unknown uncertainties," *IEEE Access*, vol. 10, pp. 103469–103484, 2022, doi: 10.1109/ACCESS.2022.3209993.

[38] J.-S. Fang, J. S.-H. Tsai, J.-J. Yan, and S.-M. Guo, "Adaptive chattering-free sliding mode control of chaotic systems with unknown input nonlinearity via smooth hyperbolic tangent function," *Math. Problems Eng.*, vol. 2019, pp. 1–9, Oct. 2019, doi: 10.1155/2019/4509674.

[39] D. N. Nguyen and T. A. Nguyen, "A novel hybrid control algorithm sliding mode-PID for the active suspension system with state multivariable," *Complexity*, vol. 2022, pp. 1–14, Jun. 2022, doi: 10.1155/2022/9527384.

[40] S. Lu, M. Lian, M. Liu, C. Cho, and C. Piao, "Adaptive fuzzy sliding mode control for electric power steering system," *J. Mech. Sci. Technol.*, vol. 31, no. 6, pp. 2643–2650, Jun. 2017, doi: 10.1007/s12206-017-0507-4.

[41] D. Lee, B. Jang, M. Han, and K.-S. Kim, "A new controller design method for an electric power steering system based on a target steering torque feedback controller," *Control Eng. Pract.*, vol. 106, Jan. 2021, Art. no. 104658, doi: 10.1016/j.conengprac.2020.104658.

[42] Y. W. Jeong, C. C. Chung, and W. Kim, "Nonlinear hybrid impedance control for steering control of rack-mounted electric power steering in autonomous vehicles," *IEEE Trans. Intell. Transp. Syst.*, vol. 21, no. 7, pp. 2956–2965, Jul. 2020, doi: 10.1109/TITS.2019.2921893.

[43] D. Jung, "A minimally configured hardware-in-the-loop simulator of electrical power steering system for human driver interaction on crosswind effect," *IEEE Access*, vol. 9, pp. 60470–60481, 2021, doi: 10.1109/ACCESS.2021.3073989.

[44] X. Ma, Y. Guo, and L. Chen, "Active disturbance rejection control for electric power steering system with assist motor variable mode," *J. Franklin Inst.*, vol. 355, no. 3, pp. 1139–1155, Feb. 2018, doi: 10.1016/j.jfranklin.2017.12.024.

[45] N. Mehrabi, J. McPhee, and N. L. Azad, "Design and evaluation of an observer-based disturbance rejection controller for electric power steering systems," *Proc. Inst. Mech. Eng., D, J. Automobile Eng.*, vol. 230, no. 7, pp. 867–884, Jun. 2016, doi: 10.1177/0954407015596275.

[46] Z. Zheng and J. Wei, "Research on active disturbance rejection control strategy of electric power steering system under extreme working conditions," *Meas. Control*, Aug. 2023, doi: 10.1177/00202940231192986.

[47] F. Wilhelm, T. Tamura, R. Fuchs, and P. Müllhaupt, "Friction compensation control for power steering," *IEEE Trans. Control Syst. Technol.*, vol. 24, no. 4, pp. 1354–1367, Jul. 2016, doi: 10.1109/TCST.2015.2483561.

[48] D. Fu, D.-Z. Li, and W.-B. Shangguan, "Model-based feedforward control for suppressing torque oscillation of electric power steering system," *Proc. Inst. Mech. Eng., D, J. Automobile Eng.*, vol. 236, nos. 10–11, pp. 2306–2317, Sep. 2022, doi: 10.1177/09544070211058347.

[49] T. Yang, "A new control framework of electric power steering system based on admittance control," *IEEE Trans. Control Syst. Technol.*, vol. 23, no. 2, pp. 762–769, Mar. 2015, doi: 10.1109/TCST.2014.2325892.

[50] J. Baek and C. Kang, "Time-delayed control for automated steering wheel tracking of electric power steering systems," *IEEE Access*, vol. 8, pp. 95457–95464, 2020, doi: 10.1109/ACCESS.2020.2990970.

[51] M. Allous, K. Mrabet, and N. Zanzouri, "Fast fault-tolerant control of electric power steering systems in the presence of actuator fault," *Proc. Inst. Mech. Eng., D, J. Automobile Eng.*, vol. 233, no. 12, pp. 3088–3097, Oct. 2019, doi: 10.1177/0954407018816556.

[52] X. Liu, H. Pang, Y. Shang, and W. Wu, "Optimal design of fault-tolerant controller for an electric power steering system with sensor failures using genetic algorithm," *Shock a*, Oct. 2018, doi: 10.1155/2018/1801589.

[53] M. Xue, G. Xu, J. Feng, C. Meizhou, and H. Xu, "Control strategy of automotive electric power steering system based on generalized internal model control," *J. Algorithms Comput. Technol.*, vol. 14, Jan. 2020, doi: 10.1177/1748302620931312.

[54] Y.-C. Hung, F.-J. Lin, J.-C. Hwang, J.-K. Chang, and K.-C. Ruan, "Wavelet fuzzy neural network with asymmetric membership function controller for electric power steering system via improved differential evolution," *IEEE Trans. Power Electron.*, vol. 30, no. 4, pp. 2350–2362, Apr. 2015, doi: 10.1109/TPEL.2014.2327693.

[55] D. Saifia, M. Chadli, H. R. Karimi, and S. Labiod, "Fuzzy control for electric power steering system with assist motor current input constraints," *J. Franklin Inst.*, vol. 352, no. 2, pp. 562–576, Feb. 2015, doi: 10.1016/j.jfranklin.2014.05.007.

[56] X. Li, X.-P. Zhao, and J. Chen, "Controller design for electric power steering system using T-S fuzzy model approach," *Int. J. Autom. Comput.*, vol. 6, no. 2, pp. 198–203, May 2009, doi: 10.1007/s11633-009-0198-0.

[57] D. Fu, S. Rakheja, W.-B. Shangguan, and H. Yin, "Robust control for fuzzy electric power steering system: A two-layer performance approach," *J. Vibrat. Control*, vol. 28, nos. 5–6, pp. 536–550, Mar. 2022, doi: 10.1177/10775463211003420.

[58] L. W. Alabe, K. Kea, Y. Han, Y. J. Min, and T. Kim, "A deep learning approach to detect anomalies in an electric power steering system," *Sensors*, vol. 22, no. 22, p. 8981, Nov. 2022, doi: 10.3390/s22228981.

[59] S. You, G. Kim, S. Lee, D. Shin, and W. Kim, "Neural approximation-based adaptive control using reinforced gain for steering wheel torque tracking of electric power steering system," *IEEE Trans. Syst., Man, Cybern., Syst.*, vol. 53, no. 7, pp. 4216–4225, Jul. 2023, doi: 10.1109/TSMC.2023.3241452.

[60] W.-Z. Zhao, C.-Y. Wang, L.-Y. Yu, and T. Chen, "Performance optimization of electric power steering based on multi-objective genetic algorithm," *J. Central South Univ.*, vol. 20, no. 1, pp. 98–104, Jan. 2013, doi: 10.1007/s11771-013-1464-4.

[61] Y. Li, G. Wu, L. Wu, and S. Chen, "Electric power steering nonlinear problem based on proportional-integral-derivative parameter self-tuning of back propagation neural network," *Proc. Inst. Mech. Eng., C, J. Mech. Eng. Sci.*, vol. 234, no. 23, pp. 4725–4736, Dec. 2020, doi: 10.1177/0954406220926549.

[62] F.-J. Lin, Y.-C. Hung, and K.-C. Ruan, "An intelligent second-order sliding-mode control for an electric power steering system using a wavelet fuzzy neural network," *IEEE Trans. Fuzzy Syst.*, vol. 22, no. 6, pp. 1598–1611, Dec. 2014, doi: 10.1109/TFUZZ.2014.2300168.

[63] C. Jie and G. Yanling, "Research on control strategy of the electric power steering system for all-terrain vehicles based on model predictive current control," *Math. Problems Eng.*, vol. 2021, pp. 1–15, Mar. 2021, doi: 10.1155/2021/6642042.

[64] W.-Z. Zhao, T. Zhao, Y.-J. Li, C.-Y. Wang, Z.-Q. Zhang, and T.-T. Duan, "Integration optimization of novel electric power steering system based on quality engineering theory," *J. Central South Univ.*, vol. 20, no. 6, pp. 1519–1526, Jun. 2013, doi: 10.1007/s11771-013-1643-3.

[65] H.-P. Chen, L.-P. Chen, and J.-M. Wang, "Model development and parameter investigation of a column-type electric power steering system," *J. Shanghai Univ.*, vol. 13, no. 6, pp. 466–473, Dec. 2009, doi: 10.1007/s11741-009-0609-2.

[66] A. Murilo, R. Rodrigues, E. L. S. Teixeira, and M. M. D. Santos, "Design of a parameterized model predictive control for electric power assisted steering," *Control Eng. Pract.*, vol. 90, pp. 331–341, Sep. 2019, doi: 10.1016/j.conengprac.2019.07.010.

[67] B. Jang, D. Lee, K. Kim, and K.-S. Kim, "Road torque modeling for electric power steering systems," *Int. J. Automot. Technol.*, vol. 23, no. 3, pp. 765–773, Jun. 2022, doi: 10.1007/s12239-022-0068-0.

[68] T. A. Nguyen, "Establishing a novel adaptive fuzzy control algorithm for an active stabilizer bar with complex automotive dynamics model," *Ain Shams Eng. J.*, vol. 15, no. 1, Jan. 2024, Art. no. 102334, doi: 10.1016/j.asej.2023.102334.

[69] A. Marouf, M. Djemai, C. Sentouh, and P. Pudlo, "A new control strategy of an electric-power-assisted steering system," *IEEE Trans. Veh. Technol.*, vol. 61, no. 8, pp. 3574–3589, Oct. 2012, doi: 10.1109/TVT.2012.2209689.

[70] T. Ayatullah and R. A. Prayoga, "On the design of electric power steering control unit," in *Proc. 5th Int. Conf. Electric Veh. Technol. (ICEVT)*, Oct. 2018, pp. 210–213, doi: 10.1109/icevt.2018.8628384.

DUC NGOC NGUYEN received the Ph.D. degree in automotive engineering from Chongqing University, in 2011. He is currently an Associate Professor with Thuyloi University, Hanoi, Vietnam. He is also the Head of the Automotive Engineering Department. He has published many international articles relating to vehicle dynamics and control.

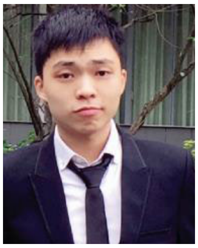

TUAN ANH NGUYEN was born in Hanoi, Vietnam, in 1995. He received the Engineering and master's degrees from the Hanoi University of Science and Technology (HUST), in 2018 and 2019, respectively. He is currently a Lecturer with the Automotive Engineering Department, Thuyloi University, Hanoi, Vietnam. He has published more than 20 international articles. His research interests include automotive engineering, vehicle dynamics, and optimization and control.